

## Research paper

# Natural mineralized fractures from the Montney-Doig unconventional reservoirs (Western Canada Sedimentary Basin): Timing and controlling factors

Marta Gasparrini<sup>a,b,\*</sup>, Olivier Lacombe<sup>c</sup>, Sébastien Rohais<sup>b</sup>, Moh Belkacemi<sup>b,c</sup>, Tristan Euzen<sup>d</sup>

<sup>a</sup> University of Milan, Earth Sciences Department, via Mangiagalli 34, Milan, 20133, Italy

<sup>b</sup> IFP Energies nouvelles, 1-4 Avenue du Bois-Préau, Rueil-Malmaison, 92852, France

<sup>c</sup> Sorbonne Université, Institut des Sciences de la Terre de Paris - IStEP, CNRS-INSU, Paris, France

<sup>d</sup> IFP Technologies (Canada) Inc., Calgary, Canada



## ARTICLE INFO

## Keywords:

Montney-Doig  
Fracture diagenesis  
Paleo-fluids  
Source rocks  
Tight reservoirs

## ABSTRACT

Characterizing the origin of natural fractures in organic-rich fine-grained deposits is key to constraining permeability evolution in these potential source rocks and tight reservoirs, as well as to assess the hydraulic connectivity of the fluid systems in which they develop.

Differently oriented calcite-filled fractures (i.e. veins), hosted by organic-rich mudrocks of the Lower-Middle Triassic Montney-Doig unconventional resource play (Western Canada Sedimentary Basin), were sampled in sub-surface well cores from British Columbia. A multidisciplinary approach (including sedimentology, Rock-Eval pyrolysis, petrography, O–C–Sr isotope geochemistry and fluid inclusion microthermometry) was applied to host-rocks and fracture filling calcites.

The results demonstrate the relevance and usefulness of such multidisciplinary studies to gather insights on: 1) the lithology-related factors controlling fracture occurrence; 2) the timing of fracture opening and the origin of the circulating paleo-fluids; 3) the openness of the fluid system through time.

More specifically, host-rock facies (particularly grain size) and vertical facies changes appear to be the leading factors controlling fracture occurrence. A less relevant role was played by the occurrence of diagenetic carbonates, while TOC possibly did not control fracture occurrence.

Three generations of calcite cemented fractures were identified. Vertical fractures (first generation) post-dated the onset of oil generation (Late Cretaceous). Horizontal, bedding-parallel fractures (second generation) post-dated the onset of gas generation and possibly opened close to maximum burial, corresponding to peak hydrocarbon (CH<sub>4</sub>) generation (Late Cretaceous - Early Paleogene). Vertical fractures (third generation) post-dated the horizontal ones and opened during basin uplift (Middle to Late Paleogene).

The consistent petrographic and geochemical features of all the calcite cements point to parent fluids in equilibrium with the host-rock lithologies, that possibly behaved as a closed hydraulic system during Late Cretaceous to Paleogene time; this would support the hypothesis that, at least in the portion of the basin investigated, the Montney Fm also acted as source rock of the unconventional system.

## 1. Introduction

Fine-grained siliciclastic deposits like shales and siltstones (i.e. mudrocks, *sensu* Lazar et al., 2015) largely contribute to the filling of sedimentary basins and most commonly constitute low-permeability rock units, unless they are affected by fracturing processes. Natural fractures commonly occur in mudrocks (e.g. Gale et al., 2014; Ukar

et al., 2017; Hooker et al., 2019), though their occurrence and the extent to which they enhance the overall rock permeability still remain poorly constrained (Dewhurst et al., 1999).

The development and sealing of natural fractures within organic-rich mudrock successions have received great attention since the interest of exploration in unconventional gas and oil plays rose, particularly in North America (Curtis, 2002; Gale et al., 2007; Engelder et al., 2009).

\* Corresponding author. University of Milan, Earth Sciences Department, via Mangiagalli 34, 20133, Milan, Italy.

E-mail address: [marta.gasparrini@unimi.it](mailto:marta.gasparrini@unimi.it) (M. Gasparrini).

<https://doi.org/10.1016/j.marpetgeo.2020.104826>

Received 5 August 2020; Received in revised form 10 November 2020; Accepted 16 November 2020

Available online 20 November 2020

0264-8172/© 2020 Elsevier Ltd. All rights reserved.

These plays encompass a variety of low-permeability reservoirs that require hydraulic fracturing to be commercially productive and are generally found within or in close association with source rock intervals. The rising interest for unconventional oil and gas plays revealed that source rocks in these settings may also represent the reservoirs of hydrocarbon (HC) accumulations which may be generated *in-situ* or may have migrated from external sources. Discriminating among the possible behaviors (open versus closed system) of organic-rich mudrock successions during burial and thermal maturation in such plays is relevant to, among others, better assess the amounts of ultimate HC in place (e.g. Jarvie et al., 2007).

On the other hand, characterizing the processes that cause natural fractures in fine-grained organic-rich deposits is crucial to better understand permeability evolution within these potential tight reservoirs (Gale and Holder, 2010; Cobbold et al., 2013; Gasparrini et al., 2014). Several mechanisms may act independently or in combination to cause fracture growth such as the conversion of organic matter in HC (Spencer, 1987; Ozkaya, 1988; Vernik, 1994; Jochum et al., 1995; Marquez and Montjoy, 1996; Zanella et al., 2014; Meng et al., 2017), the build-up of tectonic stress at different moments of the basin history (Ukar et al., 2017; Hooker et al., 2019), as well as the occurrence of specific diagenetic processes (e.g. Van de Kamp, 2008; Gasparrini et al., 2014; Hooker et al., 2017a). Regardless of the mechanisms, mineral cementation may accompany fracturing to form mineralized fracture (i.e. veins), which investigation may help discriminating fracture growth timing and/or genetic mechanism. This may be relevant for predicting evolution of hydraulic connectivity through time and joint relationships with organic matter maturation that can provide constraints to calibrate numerical models for the exploration and production of unconventional resources (e.g. Romero-Sarmiento et al., 2013; Sassi et al., 2013).

Additionally, the localization of the fractures in organic-rich mudrocks may be controlled by different factors capable of affecting the mechanical properties of the rocks (e.g. Young's modulus, Poisson's ratio). Primary sedimentary features of these deposits (e.g. grain size, total organic carbon (TOC), mineralogy), their diagenetic modifications during burial (e.g. cementations, replacements) and the vertical heterogeneities of the succession (e.g. bed thickness, facies stacking pattern, fissility), may control mechanical properties and therefore the localization of fractures and consequently, the rock response to hydraulic fracturing (e.g. Vishkai et al., 2017). However, consensus is not reached in literature on the role of these different factors (Engelder and Peacock, 2001; Rijken and Cooke, 2001; Peacock and Mann, 2005; Wang and Gale, 2009; Gale et al., 2014; Wang et al., 2016; Ilgen et al., 2017; Hooker et al., 2020; Peng et al., 2020) and this is especially true when referring to the coarser mudrock end-member, i.e. the siltstones (e.g. Vaisblat et al., 2017a; 2019; Chatellier et al., 2018).

For the different reasons mentioned above, characterizing the factors controlling the occurrence of natural fractures in organic-rich fine-grained deposits, as well as framing the timing and mechanism of fracturing within the local geological evolution, is key to evaluate permeability and fluid pathway potential through time of these rocks, and hence their present reservoir properties and sealing capacity.

Our study focuses on the mudrocks from the Lower-Middle Triassic Montney-Doig Fms in the Western Canadian Sedimentary Basin (WCSB). More specifically, the Montney Fm is one of the largest economically feasible resource plays and is classified as an unconventional tight oil and gas siltstone reservoir (Davies et al., 1997; Moslow, 2000; Euzen et al., 2018). Since the failure mechanics of such rocks is poorly understood and seldom incorporated in hydraulic fracturing or geo-mechanical models, this formation has received much attention in terms of characterization of physical and mechanical properties from laboratory tests (Ghanizadeh et al., 2015a, 2015b; Vishkai et al., 2017; Vaisblat et al., 2017a, 2019; Riazi et al., 2017; McKean and Priest, 2019). Geometric features and structural fabrics of fractures in the Montney Fm have been investigated from well cores only by few authors (Davies et al., 2014; Gillen et al., 2019). Surprisingly however, poor attention

has been paid to the characterization of the occurrence (in space and time) of natural mineralized fractures.

In an attempt at shedding new light onto these last issues, we investigated mineralized fractures occurring in the Montney-Doig lithologies from two well cores located in British Columbia by applying a multidisciplinary approach (including sedimentology, Rock-Eval pyrolysis, petrography, O–C–Sr isotope geochemistry and fluid inclusion microthermometry) to host-rocks and fracture filling calcites. The main purposes of this survey were: 1) to constrain the factors controlling fracture occurrence in relation with the host-rock properties, 2) to define the relative timing of fracture opening in the framework of the burial and geodynamic history of the WCSB, and 3) to assess the origin of the circulating paleo-waters precipitating the fracture-sealing minerals, in order to gain insight on the fluid system openness through time.

## 2. Geological setting

The WCSB is a complex, polyphase basin system the evolution of which includes a succession of rift, passive-margin basins, intracratonic and foreland basins (Mossop and Shetsen, 1994). A first collisional pro-foreland developed during the Permian, that was followed by a second stage of foreland (retro-foreland) as early as the Triassic (Ferri and Zonneveld, 2008; Golding et al., 2015; Rohais et al., 2018). Then, eastward subduction of the Farallon plate and subsequent collision of terranes along the western margin of North America during the Middle-Late Jurassic gave birth to the North American Cordillera and the associated retro-foreland basin (Price, 1994; Gillespie and Heller, 1995; DeCelles, 2004; Miall et al., 2008; Fuentes et al., 2011). Sediments were deposited in this retro-foreland basin until the Eocene (Dawson and Kalkreuth, 1994), forming an eastward-thinning wedge that is ~5–6 km thick in front of the present-day Canadian Rocky Mountains fold-and-thrust belt, and pinches out onto the Canadian Shield (Price, 1994; Wright et al., 1994; Tufano and Pietras, 2017).

The history of the WCSB has a close link to the tectonic evolution of the nearby Rocky Mountains. On the basis of radiometric age dating of gouges from major thrusts located in the Rocky Mountains and Foothills of Alberta, Pană and van der Pluijm (2015) showed that the eastward propagation of the southern Canadian Rocky Mountains fold-and-thrust belt occurred in sequence through four orogenic pulses (separated by periods of tectonic quiescence) that correspond to depositional patterns in the adjacent foreland basin. The development of the first clastic wedge in the basin was partly coeval with the initiation of the westernmost thrusts that moved during a first pulse (Late Jurassic, 163–145 Ma) in relation to the onset of thin-skinned deformation from Jurassic terrane accretion. Development of Cenomanian deltaic deposits in the basin was contemporaneous with a second thrusting pulse (mid-Cretaceous, 103–99 Ma), and the last major transgression in the southern Alberta foreland was related to a third pulse of tectonic loading (Late Cretaceous, 74–75 Ma). The outermost thrusts to the east (e.g. the McConnell thrust) moved during the last pulse (early Eocene, 52–54 Ma) and witnessed the last phase of regional contraction which triggered the accumulation of large volumes of entirely continental deposits in the foreland basin. These thrusting events presumably occurred under a NE-SW to ENE-WSW direction of the maximum principal stress  $\sigma_1$  associated to a compressional or transpressional stress regime, as revealed by paleostress analyses in the Rocky Mountains fold-and-thrust belt at the latitude of Calgary (Vandeginste et al., 2012). The stress regime later changed to extensional/transensional in type during the Eocene.

Within the WCSB, the Lower–Middle Triassic deposits of interest belong to the Montney-Doig Fms (Fig. 1) and consist primarily of fine-grained sandstones, siltstones and shales with locally occurring sandy, bioclastic packstone and grainstone beds that were accumulated in a large variety of marine (deep turbidite) to marginal-marine environments (Armitage 1962; Davies 1997; Davies et al. 1997, 2018; Zonneveld et al. 1997, 2001; Dixon 2000; Orchard and Zonneveld 2009;

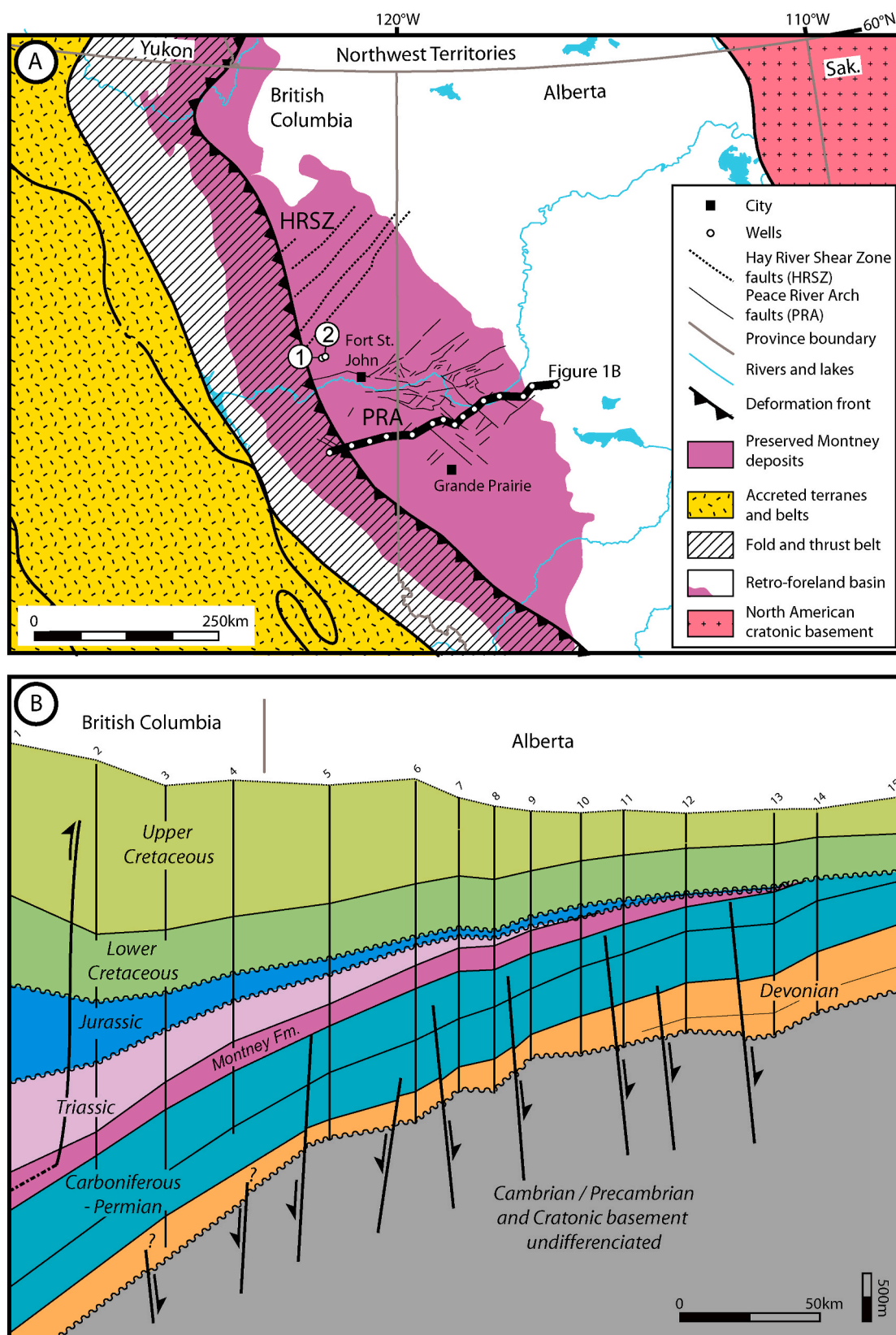


**Fig. 1.** Geographic and geological setting of the study area. **A.** Geological map of the Canadian segment of the Cordillera including the main belts and terranes, and the Western Canada Sedimentary Basin (WCSB). The purple color shows the subcrop and outcrop areas where Triassic deposits are still preserved (simplified from Rohais et al., 2018 and references herein). The Hay River Shear Zone (HRSZ) and the inherited structure from the Paleozoic Peace River Arch (PRA) collapse are highlighted as main structural elements below the Triassic strata. (1) and (2) refer to the location of the wells investigated, localized in between these two main structural domains. The black dotted line represents the trace of a cross-section (illustrated in B). **B.** Cross-section of the WCSB illustrating the main stratigraphic intervals and the faults (simplified from Ducros et al., 2017). (For interpretation of the references to color in this figure legend, the reader is referred to the Web version of this article.)

Crombez et al., 2016; Moslow et al., 2016, 2018; Furlong et al., 2018a; Euzen et al., 2018; Sanders et al., 2018; Zonneveld and Moslow, 2018). This sedimentary succession was initially sub-divided into three formations, from older to younger: the Montney, Doig and Halfway, with a recent update between the Montney and Doig Fms corresponding to the localized Sunset Prairie Fm (Furlong et al., 2018b). The Lower-Middle Triassic deposits are preserved in between the Permian Belloy Fm and the Late Triassic Charlie Lake Fm or the regional pre-Cretaceous erosional unconformity. The Lower-Middle Triassic deposits were affected by reactivation of inherited structures from both the Paleozoic Peace River Arch (PRA) collapse, and the older Hay River Shear Zone (HRSZ) (Fig. 1; Davies, 1997; Peirce et al., 2001).

The synthetic stratigraphic architecture of the Montney-Doig interval (Crombez et al., 2019) is presented in Fig. 2. Four sequence boundaries are presented, delimiting four third order stratigraphic sequences. The first three (sequences 1–3) belong to the Montney Fm, and the last (sequence 4) encompasses the Doig and Halfway Fms. This study is mainly focused on the three sequences of the Montney Fm (sequences 1–3), and on the basal part of the sequence 4 including the Doig Phosphatic Member (Doig Fm).

Triassic source rocks only reach maturity in the western part of the WCSB and become overmature close to the Cordillera deformation front. The peak HC generation ranges from approximately 100 Ma (mid-Albian) to 60 Ma (Paleocene) for the Doig Fm based on 1D basin modeling (Ness, 2001). According to Ness (2001), the timing of HC generation for the Montney Fm is more complex with possible early generation between 120 and 130 Ma, and additional later oil and gas generation during burial at approximately 100–110 Ma. At basin scale, secondary gas generation probably started at 90–100 Ma and at about 70 Ma in the studied sector (Ness, 2001). More recently, Ducros et al. (2017), based on 2D petroleum basin modeling, suggested that the Montney Fm started to generate HC in this western part of the basin during the Late Cretaceous (88,5 Ma). These authors also suggested that the Montney Fm reached the maximum transformation rate just before reaching the maximum burial, which was followed by a major exhumation and erosional event starting in the Early Paleogene.

### 3. Material and methods

Two non-oriented well cores from British Columbia (ca. 70 Km North-West of Fort St. John; Fig. 1A) intercepting the Montney and Doig Fms were investigated. They correspond to 00/16-17-083-25W6/0 and to 00/12-36-083-25W6/0, vertical wells (BC Oil & Gas Commission), hereafter referred as 16–17 and 12–36, respectively. The wells are

located ca. 70 km North-West of Fort St. John and between the HRSZ and the inherited structure from the Paleozoic PRA collapse (Fig. 1A). They are located 7.2 km from each other and based on available basin models (see later in this section) have experienced a similar burial and thermal history. In particular, the 16–17 continuous well core includes the entire section of the Montney Fm (sequences 1, 2 and 3; Crombez et al., 2016) and the basal part of the Doig Fm, whereas the 12–36 well core is composed of three discontinuous cores of the Montney Fm only for which mineralogical data for two of them (core 1 and core 3) are available from the British Columbia Oil & Gas Commission public database.

Sedimentological logs for the two well cores were described at the 1:50 scale by some of the co-authors in the frame of a PhD thesis (Crombez, 2016). Wire-log data for the two well cores were available from the British Columbia Oil & Gas Commission. Investigated well core depth goes from 2531 to 2233 m for well 16–17 and from 2369 to 2088 m for well 12–36. Lithology, sedimentary structures, textures and paleontological contents allowed characterizing different macro-facies. Occurrence and orientation of fractures was also reported on the logs (Fig. 3). The majority of the observed fractures are cemented by calcite (and will be here referred as veins), though a few non-mineralized fractures also occur.

Descriptive properties derived from macroscopic observations (i.e. facies, depositional environment, occurrence of differently oriented fractures) and analyses (i.e. TOC) of the two studied well cores were classed and converted into numerical codes (Table 1). Points were continuously sampled along the two logs and Excel spreadsheets were completed with the information on the different properties (Table S3a and Table S3b of the Supplementary Material). A total of 232 and 576 points were sampled on the logs for well cores 12–36 and 16–17, respectively. These spreadsheets served as input in the EasyTrace™ software in order to convert the original descriptive information into a quantitative dataset to achieve frequency distribution analysis of the different properties (see details on this approach in Gasparrini et al., 2017). Using EasyTrace™ multivariate statistical analysis with the compiled spreadsheets enabled us to highlight the link between the type of depositional facies (with their TOC) and the occurrence and orientation of the fractures, as well as the fracture distribution within the different stratigraphic sequences of the studied formations.

Fifty samples, mostly containing mineralized fractures were collected from the two studied wells (23 from 16-17 and 27 from 12-36). The samples were used to make thin polished and thick double-polished sections for petrographic, geochemical and fluid inclusion studies. The vein host-rock from these samples was milled and analyzed with Rock-

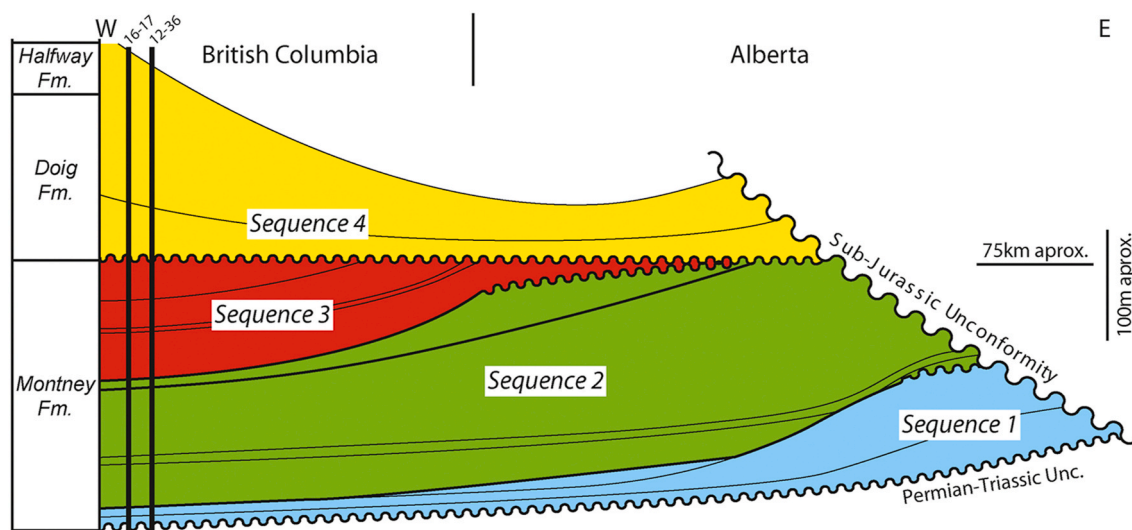
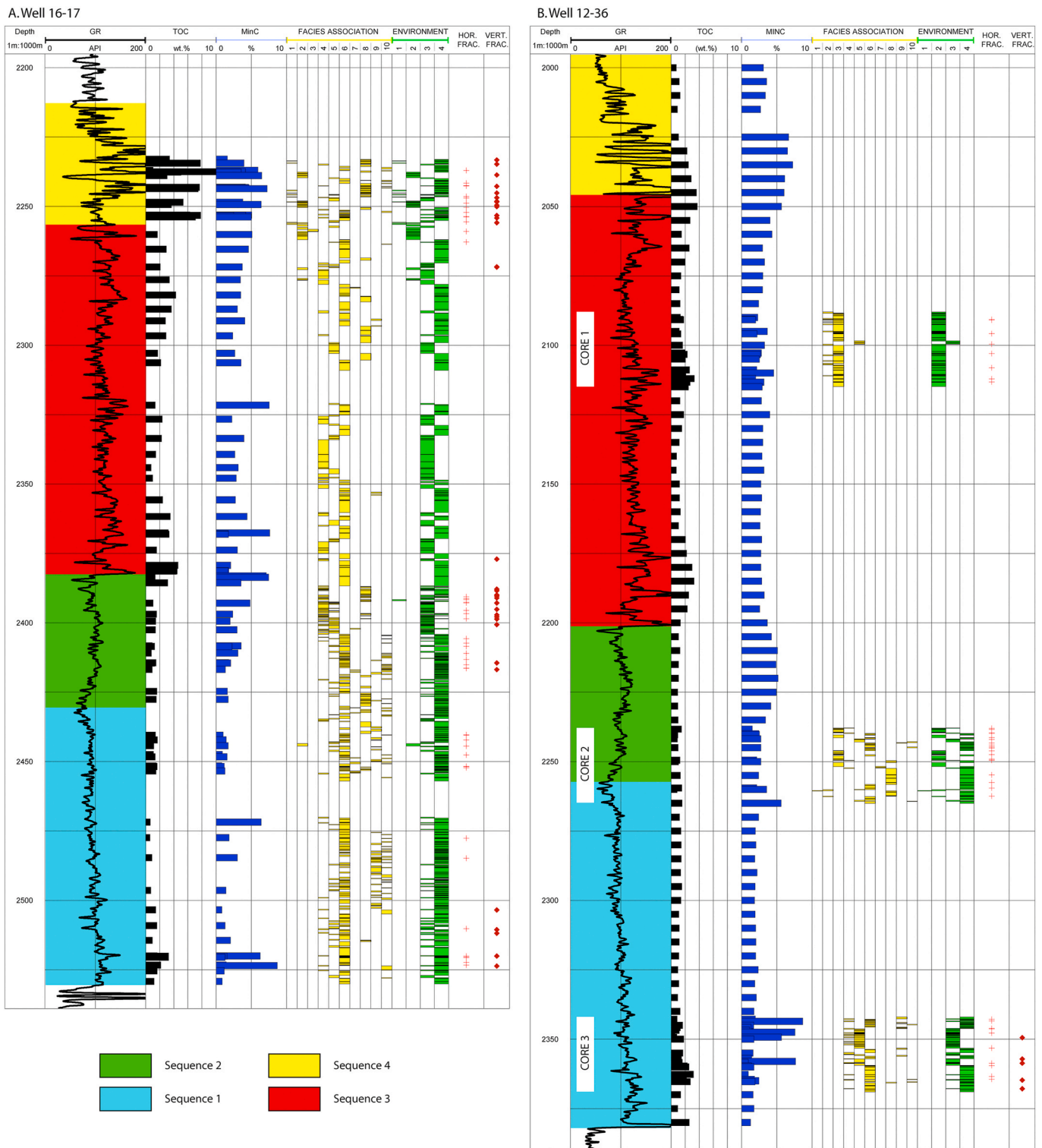


Fig. 2. Simplified sedimentary architecture and main stratigraphic sequences of the Lower and Middle Triassic of the WCSB (modified after Crombez et al., 2019).



**Fig. 3.** Simplified stratigraphy of the two investigated wells including the gamma ray response and sequences of the studied succession, the TOC and MinC from Rock-Eval (by merging data from this study and from [Crombez et al., 2016](#)), the facies associations (in yellow) and their interpretation in terms of depositional environments (in green), as well as the location of the observed fractures with their orientation. See [Table 1](#) for the legend of numerical codes used to define the different facies associations and depositional environments. (For interpretation of the references to color in this figure legend, the reader is referred to the Web version of this article.)

Eval 6 pyrolysis. Here follow the details on the different methodologies and apparatus used.

Thirty-seven polished thin sections (30–35 μm thick) were prepared for conventional and cathodoluminescence (CL) microscopy, as well as for staining. Thin section petrography was performed on a Nikon

ECLIPSE LV100 POL equipped with a mercury vapor lamp (100 W), allowing UV-light observations. Calcite crystal habitus and crystal spatial arrangement (texture) in the fractures were described using the terminology suggested by [Bons et al. \(2012\)](#) and [Woodcock et al. \(2007\)](#). For samples affected by dolomitization the dolomite texture

**Table 1**

Tables summarizing the codes attributed to the main properties (i.e. sequences, facies associations, depositional environments, fracture occurrence) recorded along the logs of the studied well cores. These codes were used for frequency distribution analysis with EasyTrace™ software.

FACIES ASSOCIATION	Code	SEQUENCE	Code	TOC	Code
Lag	1	Sequence 1	1	<1	1
Massive fine-grained sandstones	2	Sequence 2	2	between 1 and 2	2
Massive vf-grained ss. to siltstones	3	Sequence 3	3	between 2 and 3	3
Sand-dominated alternation	4	Sequence 4	4	between 3 and 4	4
Silt-dominated alternation	5			between 4 and 5	5
Massive siltstones	6	<b>ENVIRONMENT</b>	<b>Code</b>	between 5 and 11	6
Organic-rich siltstones	7				
Bioclastic siltstones	8	Lag	1	<b>FRACTURE</b>	<b>Code</b>
Laminated siltstones (turbidite)	9	Shoreface	2		
Laminated siltstones	10	Offshore transition	3	no fracture	1
		Offshore	4	horizontal	2
				vertical to high angle	3

classification from Sibley and Gregg (1987) was used. The cold-cathode CL device used is a 8200 Mk5-2 (CITL) which was employed under vacuum (<0.1 mBar) and with 250 μA and 10 kV operating conditions. A portion of all thin sections was stained with a solution composed of diluted HCl (10%) with Alizarin red -S and potassium ferricyanide to distinguish calcite from dolomite and qualitatively estimate their Fe content (Dickson, 1966).

Seven double-polished thick sections (100–120 μm thick) were prepared for Fluid Inclusion (FI) petrography and microthermometry measurements. Different FI assemblages were distinguished based on their location within the crystals, e.g. crystal cores, growth zones, along trails, isolated. For bi-phase FIs, the volumetric proportion of the liquid phase relative to the total volume of the FI, referred as degree of fill (F), was calculated at room temperature from 2D screen images by

measuring areas. Microthermometry was carried out with a Linkam MDS 600 stage mounted on a Nikon LV100 Eclipse, with a 100 W Mercury vapor lamp which allowed UV-light observations. The stage was calibrated with synthetic FIs in the temperature range -56.6 to +135 °C. The Linksys 32 software enabled all the operations for FI microthermometry. The measurement accuracy was of 1 and 0.2 °C for heating and cooling runs, respectively. For aqueous fluids, heating runs were accomplished before cooling runs. Salinities were calculated from final melting of ice (Tmi) in the binary H<sub>2</sub>O–NaCl system (Bodnar, 1993). Oil density was qualitatively estimated from fluorescence color of hydrocarbon FIs based on the chart from Mclimans (1987).

Carbonate (calcite) powders from the targeted veins were extracted from polished rock slabs by means of a dental drill to be analyzed for oxygen (O), carbon (C) and strontium (Sr) isotopes.

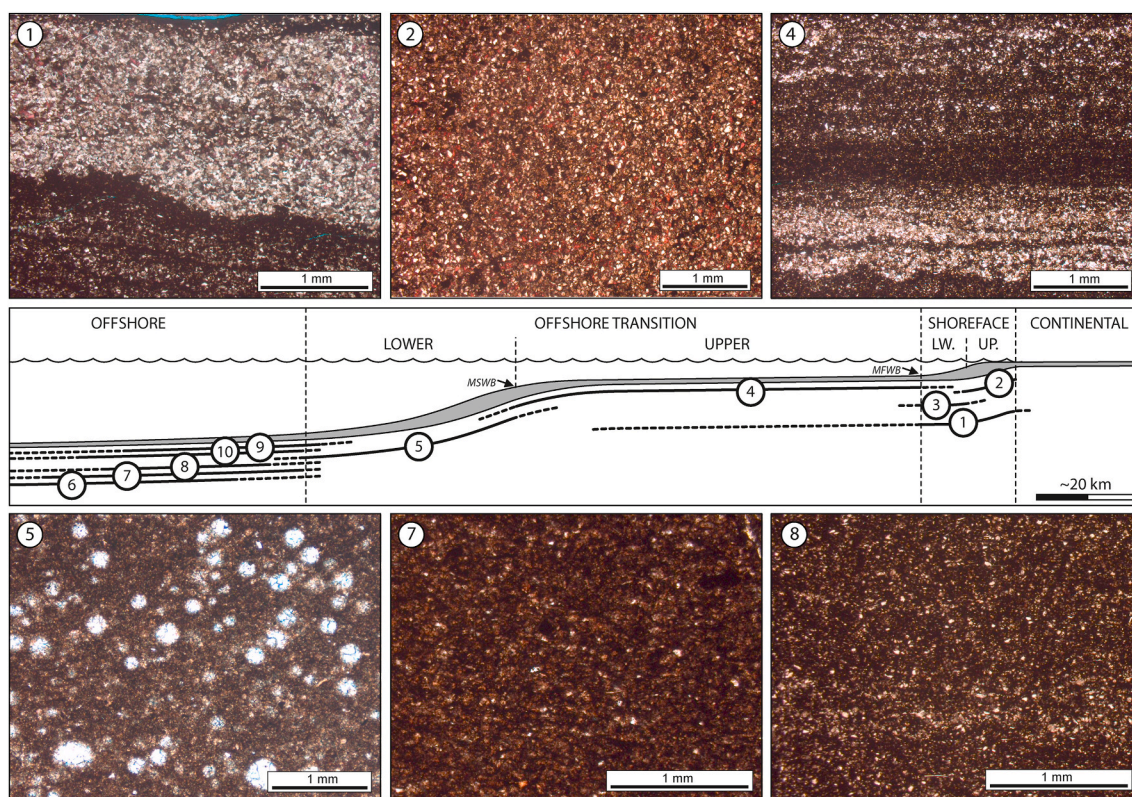


**Fig. 4.** Reconstructed depositional profile for the Montney-Doig interval with main facies associations and microfacies petrographic images (in PPL) for some of them. 1. Lag; 2. Massive fine-grained sandstones; 3. Massive very fine-grained sandstones to siltstones; 4. Sand-dominated alternation of very fine-grained sandstones to siltstones; 5. Silt-dominated alternation of very fine-grained sandstones to siltstones; 6. Massive siltstones; 7. Organic-rich massive siltstones; 8. Bioclastic siltstones; 9. Laminated siltstones with mm-thick sand laminae (low density turbidite); 10. Laminated siltstones.

**Table 2**

Range and mean TOC and HI values from bulk-rock Rock-Eval measurements for the investigated samples by sequence and well core of belonging.

Stratigraphic sequence	Core 16–17				Core 12–36			
	TOC (%)		HI (mgHI/gTOC)		TOC (%)		HI (mgHI/gTOC)	
	range	mean	range	mean	range	mean	range	mean
4	1.1–6.6	3.7	11.0–27.0	19.3				
3	1.3–1.4	1.3	14.0–15.0	14.5	1.4–3.3	2.2	29.0–39.0	34.0
2	0.8–1.6	1.2	8.0–10.0	9.0	0.9–2.5	1.2	16.0–24.0	20.0
1	0.8–3.3	16.0	5.0–9.0	7.3	0.6–3.3	1.5	9.0–23.0	14.7

Forty-one calcite powders were analyzed for O and C isotopes. The samples were reacted with 100% phosphoric acid at 70 °C up to 7 h. A Gasbench II connected to a Thermo Finnigan Five Plus mass spectrometer was used. All values for carbonate phases are reported in per mil relative to V-PDB by assigning a  $\delta^{18}\text{O}$  value of  $-2.20\text{‰}$  and a  $\delta^{13}\text{C}$  value of  $+1.95\text{‰}$  to the NBS19 standard. Reproducibility was checked by replicate analysis and is better than  $\pm 0.07\text{‰}$  for  $\delta^{18}\text{O}$  and  $\pm 0.06\text{‰}$  for  $\delta^{13}\text{C}$  (1 std. dev).

Eleven calcite powders were also analyzed for Sr isotopes. Carbonate samples were leached in ammonium acetate to remove groundwater salts and displace contaminant Sr on exchangeable sites (e.g. Bailey et al., 2000). The remaining material was rinsed twice in deionized water, and then dissolved in dilute HCl. After ion exchange chemistry, samples were loaded onto purified Re filaments in a Ta emitter solution (Birck, 1986). Isotopic analyses were made on a VG-Sector-54 thermal ionization mass spectrometer using a three cycle dynamic multicollector routine and an exponential mass fractionation correction relative to  $^{86}\text{Sr}/^{88}\text{Sr} = 0.1194$  (e.g. Hans et al., 2013). Repeated measurements of reference material NBS987 at similar run conditions during the period over which the analyses were made yielded a value indicating that the measurement repeatability is commensurate with the within-run uncertainty.

The Rock-Eval 6 pyrolysis apparatus was used to calculate, among other parameters, the TOC, the Hydrogen Index (HI) and the Mineral Carbon (MinC) of 46 fracture host-rock samples. The Shale Play Method® developed at IFP Energies nouvelles (Behar et al., 2001; Romero-Sarmiento et al. 2016a, 2016b) was used on bulk-rock samples, allowing for a better estimate of the free or absorbed HC in the rocks. 50–70 mg of powdered sample is heated in an open pyrolysis system under non-isothermal condition (from 300 to 650 °C). During this pyrolysis, the amount of HC released is measured by a flame ionization detector (FID) and CO and CO<sub>2</sub> release are monitored with an infrared (IR) detector. The residual sample is then put in an oxidation oven where it is heated (from 300 to 800 °C) under artificial air (N<sub>2</sub>/O<sub>2</sub>: 80/20).

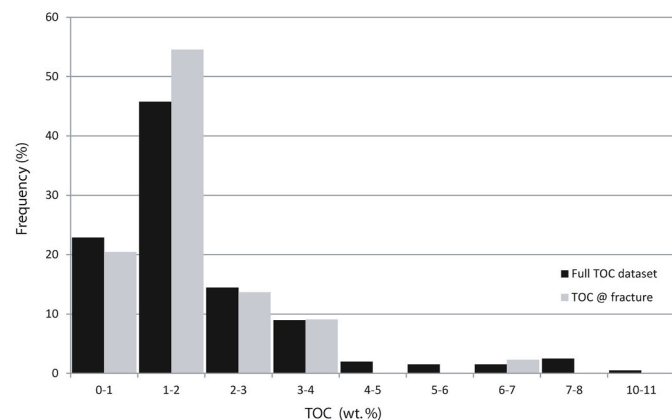


**Fig. 5.** Frequency distribution of TOC values (in wt. %) from the two investigated wells according to two different datasets: 1) continuous sampling of cores and cuttings from Crombez et al. (2016), in black; 2) core samples hosting fractures from this study, in grey.

During combustion, the amount of CO and CO<sub>2</sub> released are monitored with an IR detector.

In addition, among the 46 bulk-rock samples analyzed, 10 samples were selected for organic solvent extraction. The powdered samples were placed in a solution of dichloromethane and methanol (1/1) in an ultrasonic bath at 40 °C for 30 min. The samples were then filtered and placed in a drying oven for one day. Finally, the samples of extracted organic matter were analyzed again by using the Shale Play Method® of the Rock-Eval 6 apparatus described above.

A 3D basin model under TemisFlow™ software available in-house was used to estimate the thermo-barometric evolution of the studied stratigraphic interval with time. In this basin model a constant heat flow of 47 mW/m<sup>2</sup>, and then 57 mW/m<sup>2</sup> was imposed at the base of the sedimentary pile, based on a lithospheric model, and thermal calibration was achieved by making use of vitrinite reflectance data to test the two heating scenarios (Pauthier et al., 2016; Ducros et al., 2017). This model takes into account the amplitude of the Tertiary uplift, with an estimated thickness of eroded sediments that ranges from 4000 m close to the Rocky Mountains (Roure et al., 2010) to less than 400 m near the Precambrian shield in Saskatchewan (Ness, 2001; Higley et al., 2005; Roure et al., 2010).

## 4. Results

The main results from well core logging, facies analysis and stratigraphy are reported in Fig. 3 together with the TOC and MinC from Rock-Eval pyrolysis and the location and orientation of the fractures. Table S1a and Table S1b (see Supplementary Material) summarize details on the samples collected from wells 16–17 and 12–36, respectively, together with the sample depth, sequence of provenance, fracture orientation and kinematic aperture, petrography of the calcite sealing cements and their O–C isotope composition. Table S2a and Table S2b (see Supplementary Material) report the results of Rock-Eval pyrolysis for the rock samples hosting the fractures (on bulk-rock and extracted organic matter, respectively) for the two well cores investigated. Finally, Table S3a and Table S3b (see Supplementary Material) report the data-sheets with the evolution of the different properties with depth, used for frequency distribution analysis with Easytrace™ software.

### 4.1. Sedimentology

In this contribution, we primarily refer to detailed descriptions of the sedimentary facies previously published (Crombez et al., 2016; Playter et al., 2018). The two studied wells are located in the distal area of the WCSB where a narrow range of grain size and a dolomitic-feldspathic composition is expected to dominate the Montney lithologies, as due to arid climate conditions during deposition (e.g. Euzen et al., 2020; Zonneveld and Moslow, 2018). They contain relatively hard grains (e.g. quartz, feldspars, carbonates), moderate amounts of organic matter and, variable content of clay minerals (e.g. Euzen et al., 2018; Vaisblat, 2020). Indeed, clay content is overall low (<15%) except in Sequence 1 (up to 25%; Euzen et al., 2015).

Petrographic observations on thin sections indicate that the investigated samples have grain size from very fine sandstone to fine siltstone, locally with clays. In particular, the Montney samples are often

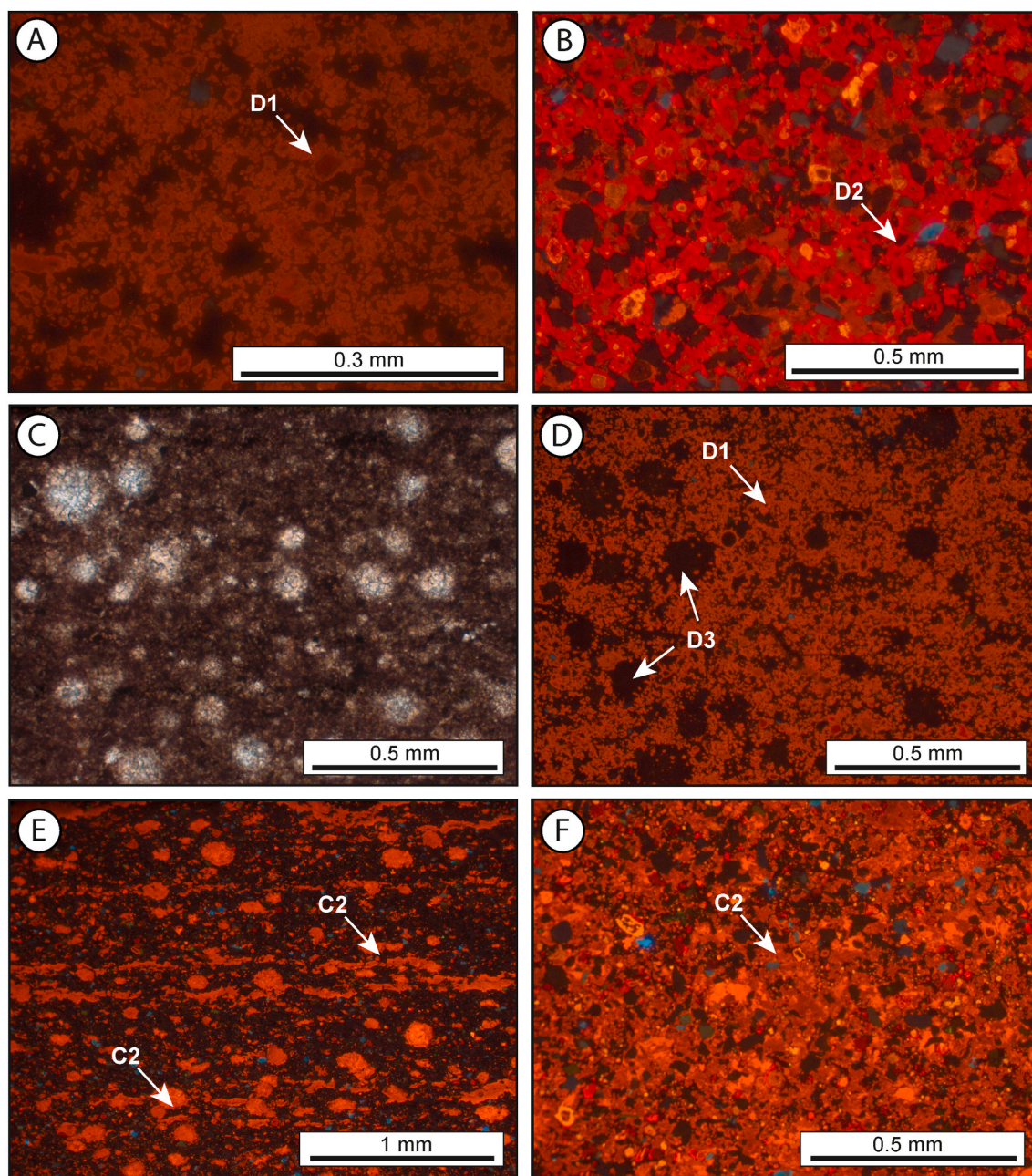


**Fig. 6.** Photomicrographs illustrating the main carbonate diagenetic phases occurring in the studied samples of the Montney-Doig Fms. **A.** Euhedral to sub-hedral D1 crystals with dull orange CL totally or partially replacing detrital dolomite grains (sample 16-17-21). **B.** D2 crystals with bright red CL locally forming overgrowths around detrital grains locally replaced by D1 (sample 16-17-23). **C.** Facies with calcispheres from the offshore environment (sample 16-17-21). PPL. **D.** Same image of C. under CL. Calcispheres are replaced by the ferroan and non-luminescent D3. **E.** C2 crystals with bright orange CL occurs as cement in intergranular pores or as replacement of calcispheres (sample 1236-C3-6). **F.** C2 with bright orange CL occurs as cement in intergranular pores or replaces previous carbonate phases (sample 1617-15). PPL = plane polarized light, CL = cathodo luminescence. (For interpretation of the references to color in this figure legend, the reader is referred to the Web version of this article.)

characterized by consistent grain size with silt-sized particles of 10–25  $\mu\text{m}$  being dominant, locally with very fine sands (<80  $\mu\text{m}$ ), whereas the more clay-rich intervals could not be further characterized due to the limited resolution of the conventional optical microscopy used. This dataset allows to consider the studied lithologies as mudrocks, according to the definition of Lazar et al. (2015) which includes silt-sized particles (fine mud <8  $\mu\text{m}$ , medium mud = 8–32  $\mu\text{m}$  and coarse mud = 32–64  $\mu\text{m}$ ). In this contribution, we primarily refer to detailed descriptions of the sedimentary facies previously published (Crombez et al., 2016; Playter et al., 2018). Ten facies associations were identified (Figs. 3 and 4) by conducting a higher resolution lithology and facies analysis

combined with the microfacies analysis from thin section petrography: 1. Lag; 2. Massive fine-grained sandstones; 3. Massive very fine-grained sandstones to siltstones; 4. Sand-dominated alternation of very fine-grained sandstones to siltstones; 5. Silt-dominated alternation of very fine-grained sandstones to siltstones; 6. Massive siltstones; 7. Organic-rich massive siltstones; 8. Bioclastic siltstones; 9. Laminated siltstones with mm-thick sand laminae (low density turbidite); 10. Laminated siltstones.

The ten facies associations identified were then grouped into four main depositional environments: (1) lag, (2) shoreface, (3) offshore transition, (4) offshore. Given the distal position of the wells in the



basin, the very proximal depositional environments (e.g. foreshore or tidal) were not encountered. Lag deposits do not strictly represent a depositional environment since they are rather related to erosional and reworking processes influenced either by wave-, or storm-action.

#### 4.2. Rock-Eval pyrolysis

The Montney and Doig Fms contain organic matter of type II and III (Crombez et al., 2016; Riediger, 1997; Romero-Sarmiento et al., 2016b). The mean TOC is in the range 0.5% - 4 wt% and up to 8.2 wt% TOC in the Montney Fm, and may reach 11% in the Doig Fm within the Doig Phosphatic Member at the base (Riediger et al., 1990a; Ibrahimbas and Riediger, 2004; Crombez et al., 2016; Romero-Sarmiento et al., 2016b).

Table 2 illustrates the mean TOC and HI values for the 46 fracture host-rock samples analyzed in this study by stratigraphic sequence and by well. The complete dataset acquired in the present study by Rock-Eval analysis is reported in Table S2a and Table S2b (see Supplementary Material).

The studied 46 samples have TOC between 0.56 and 6.65% (mean is 1.74%) with only 13% of the samples having TOC above 3.00%. In particular, a mean TOC of 1.68% is recorded from the 26 samples of 12–36 well, whereas a mean of 1.91% is recorded from the 20 samples of 16–17 well; the highest value of 6.65% is recorded in 16–17 well at the TST of sequence 4, corresponding to the Doig Phosphatic Member.

All samples analyzed here display HI below 50 mgHC/gTOC, pointing towards a low hydrocarbon potential, possibly due to the fact that maturation in the studied intervals has already occurred.

The pyrolysis results obtained from the 10 samples analyzed twice (i. e. on bulk-rock and on extracted organic matter) were compared. The procedure of organic matter extraction eliminated all the light HC (free and adsorbed) and part of the heavy and very heavy HC. The TOC values obtained on bulk-rock and extracted organic matter are similar (see Table S2a and Table S2b in Supplementary Material), suggesting that only the carbon from organic matter contributes to the TOC computation. This ensures the reliability of the TOC values from the remaining 36 samples which were analyzed on the bulk rock only.

Crombez et al. (2016) previously published TOC and MinC values from continuously sampled cores and cuttings (155 samples) of the same wells. Measurements were done by means of the same Rock-Eval 6 apparatus, though by using the classic method (Lafargue et al., 1998; Behar et al., 2001). TOC values measured by these previous authors were compared to those measured on close samples during this study for a quality check; the values from the two independently obtained datasets mostly overlap, the TOC difference being within the uncertainty range. This also confirms that the classic and the Shale Play Method® of the Rock-Eval 6 apparatus lead to equivalent TOC computation (as already underlined by Romero-Sarmiento et al., 2016a; 2016b).

Fig. 5 reports the frequency distribution of the available TOC data (in wt. %) by comparing the values measured in this study (on fracture host-rock samples only) with the full dataset by also including the values measured by Crombez et al. (2016). The figure illustrates that the two TOC datasets have an overlapping distribution, the only minor difference being that in our dataset samples with TOC of 1–2 wt % are more represented. This suggests that the TOC data at fractures here produced is representative of the whole TOC dataset available for the studied well cores.

#### 4.3. Host-rock diagenesis

Thin section optical petrography combined with CL observations of the fracture host-rocks revealed that several diagenetic events affected the studied formations after deposition. The study was focused on the carbonate diagenetic phases occurring as cements or replacements, therefore potentially affecting the rock mechanical properties. Here follow the details on the main diagenetic phases observed.

A first calcite (C1) may pervasively cement the most proximal

(bioclastic) samples by filling the intergranular pores between bioclasts. It is composed of non-ferroan calcite crystals (10–60 µm) displaying a uniform and bright orange response under CL. It is rarely observed and is considered of minor extent in the studied wells.

A first dolomite (D1) may totally or partially replace the detrital carbonate grains. It consists of non-ferroan euhedral to sub-hedral crystals (10–30 µm), building up a planar-E texture and displaying a uniform to zoned dull orange to dull red CL (Fig. 6A).

These first two phases (C1 and D1) are interpreted to have precipitated during eogenesis (early burial diagenesis) because of their non-ferroan nature. Furthermore, samples affected by C1 cementation lack major mechanical compaction features, suggesting that C1 precipitation occurred before significant burial.

Mechanical compaction is witnessed in many samples by micro-fracturing of bioclasts, as well as by the presence of grain to grain (locally interpenetrated) contacts.

A second dolomite (D2) mainly occurs as a cement since it forms overgrowths (5–10 µm thick) around detrital carbonate grains commonly replaced by D1 (Fig. 6B), although locally it also replaces the carbonate grains. It is composed of ferroan dolomite crystals showing a uniform to zoned bright red CL (Fig. 6B).

A third dolomite (D3) may totally replace specific bioclasts like the calcispheres (Fig. 6C). It consists of ferroan anhedral crystals (10–50 µm), which make up a non-planar texture, do not luminesce under CL (Fig. 6D) and acquire a deep blue color after staining.

The ferroan nature of these latter two dolomite phases (D2 and D3) points towards a precipitation during mesogenesis, in the late burial environment, where reduced Fe<sup>2+</sup> may commonly be available for uptake into the carbonate lattice upon crystallization.

A second calcite (C2) phase mainly occurs as a cement within intergranular pores. It consists of non-ferroan granular to blocky crystals (10–50 µm) with a uniform bright orange luminescence. It possibly precipitated after major mechanical compaction as suggested by the presence of compaction features (e.g. grain to grain interpenetrated contacts) in samples pervasively affected by C2 cementation. C2 may also occur as a replacement of previously precipitated carbonate phases (Fig. 6E and F).

Pyrite occurs in all samples both as small framboids (<5–10 µm) or in large euhedral crystals (10–50 µm). It replaces mainly the bioclasts and the early diagenetic calcites but also the third (ferroan) dolomite (D3) occurring within calcispheres.

Some of the above diagenetic phases may preferentially occur in facies from one or more depositional environments. For instance, the first dolomite (D1; eogenetic replacement) is observed only in samples from the 16–17 well, mainly from the shoreface environment and secondarily from the offshore transition environment. Furthermore, the third dolomite (D3; burial replacement) always occurs in facies containing calcispheres which are dominantly found in samples from the offshore transition and the offshore environments. The other diagenetic phases described above do not seem to be facies specific and are observed in similar proportions in all of the identified depositional environments.

Diagenesis studies on the Montney Fm were conducted by previous authors (Vaisblat et al., 2017b; Vaisblat 2020). Vaisblat et al. (2017b) investigated 83 samples coming from two wells located in British Columbia for petrography (SEM), mineralogy (XRD) and geochemistry (QEMSCAN). In particular, 68 samples out of the 83 come from well 16–17, also investigated in the present study. Our observations (though based on optical petrography and CL only) were therefore compared with those of Vaisblat et al. (2017b); the main differences are illustrated in Fig. 7. This comparison reveals that in the present study authigenic clay minerals, quartz cement and feldspar dissolution/precipitation were not observed, due to the limited resolution of the conventional optical microscopy. On the other hand, some carbonate phases were here documented for the first time (Fig. 6); these are the non-ferroan first calcite (C1) and first dolomite (D1) phases, precipitated during

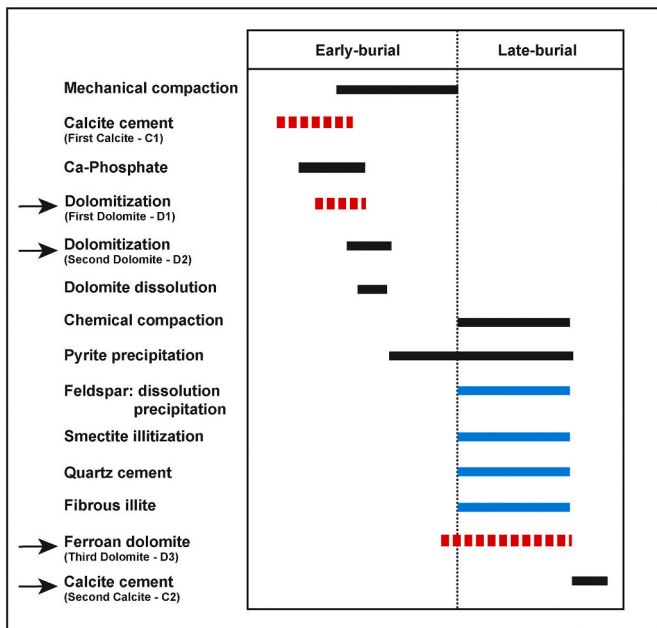


**Fig. 7.** Paragenetic sequence reconstructed for the Montney-Doig Fms in this study as compared with the one from Vaisblat et al. (2017b). In black the phases that were observed in both studies; in blue the phases that were observed only by Vaisblat et al. (2017b); in red the phases that were observed only in this study. Black arrows indicate the four most abundant carbonate diagenetic phases. (For interpretation of the references to color in this figure legend, the reader is referred to the Web version of this article.)

eogenesis and the ferroan third dolomite (D3), precipitated during burial within calcispheres.

Interestingly, no diagenetic sulfates were detected in the Montney-Doig lithologies of the studied well cores, in contrast with the observations made in well cores located further to the south (Liseroudi et al., 2020), i.e. within the inherited structure from the Paleozoic PRA collapse (Fig. 1A).

#### 4.4. Fracture orientation and abundance

All the fractures (both mineralized and non-mineralized) observed along the 16–17 and 12–36 vertical well cores were reported on the sedimentological logs. Macroscopically, the fractures were classified

according to their orientation (Fig. 8): horizontal (bedding-parallel) or vertical (vertical s.s. or at high angle to bedding). The persistence of the vertical to high angle fractures mostly ranges from 3 to 10 cm and only rarely exceeds 20 cm; the persistence of the horizontal fractures could not be estimated since it exceeds the core width.

For the properties recorded on the sedimentological logs (i.e. facies associations, depositional environments, stratigraphic sequences, occurrence and orientation of the fractures) and for those measured in the laboratory (i.e. TOC) different classes were established and expressed by means of numerical codes (Table 1).

The complete spreadsheets used for statistical treatment with Easy-Trace™ software are reported in Table S3a and Table S3b (see Supplementary Material) for wells 16–17 and 12–36, respectively. The treatment of these data highlighted different possible correlations between the abundance and orientation of the fractures and the host-rock features as well as their distribution within the four stratigraphic sequences (Fig. 9).

The 10 facies associations (property here referred to as FACIES) previously identified (Figs. 3 and 4) were grouped into four broad depositional environments (property here referred as ENVIRONMENT) as follows: the lag (code 1), the shoreface (code 2) which groups the facies associations 2 and 3, the offshore transition (code 3) which groups the facies associations 4 and 5 and the offshore (code 4) which groups the facies associations 6, 7, 8, 9 and 10 (see Table 1).

The four stratigraphic sequences (property here referred to as SEQUENCE) of the studied formations were classed from 1 to 4 (Table 1) as follows: sequence 1 (code 1), sequence 2 (code 2), sequence 3 (code 3), sequence 4 (code 4).

The TOC contents (property here referred as TOC) from fracture host-rock samples analyzed in this study (Table 2 and Fig. 5) were classed from 1 to 6 (Table 1) as follows: <1% (code 1), 1–2% (code 2), 2–3% (code 3), 3–4% (code 4), 4–5% (code 5), 5–11% (code 6).

Finally, the presence/absence of fractures and their orientation along the logs (property here referred as FRACTURE) were classed by means of 3 codes (Table 1) as follows: no fracture occurrence (code 1), occurrence of horizontal fractures (code 2), occurrence of vertical to high angle fractures (code 3).

Fig. 9 illustrates the results of the statistical treatment with Easy-Trace™ software for the two wells. The red lines represent the distribution of the whole sampled points where fractures occur (i.e. only the points with codes 2 and 3 of the property FRACTURE). Fig. 9A and B shows respectively the distribution of sampled points characterized by the presence of horizontal and vertical to high angle fractures; the black bars indicate in which SEQUENCE, ENVIRONMENT and TOC classes fall

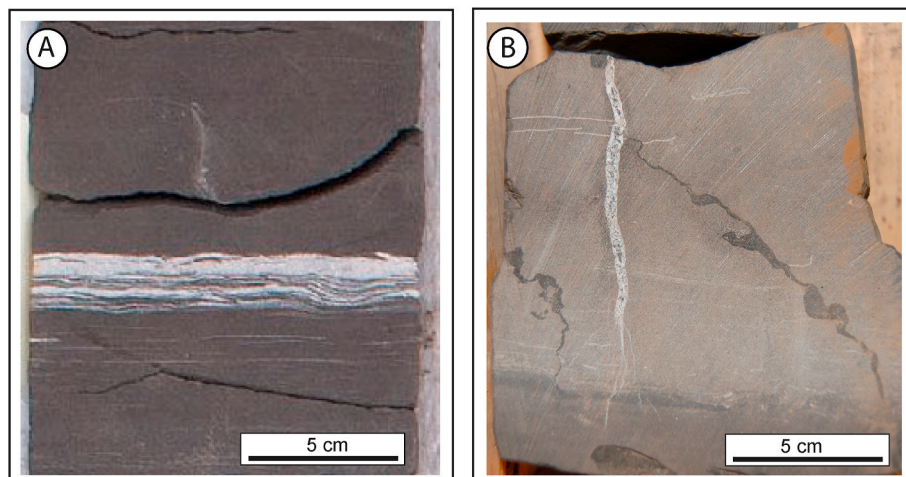


**Fig. 8.** Well core pieces containing macroscopically visible mineralized fractures (i.e. veins). A. Horizontal vein from well 12–36 at 2364.3 m of depth. B. Vertical vein from well 16–17 at 2350 m of depth.

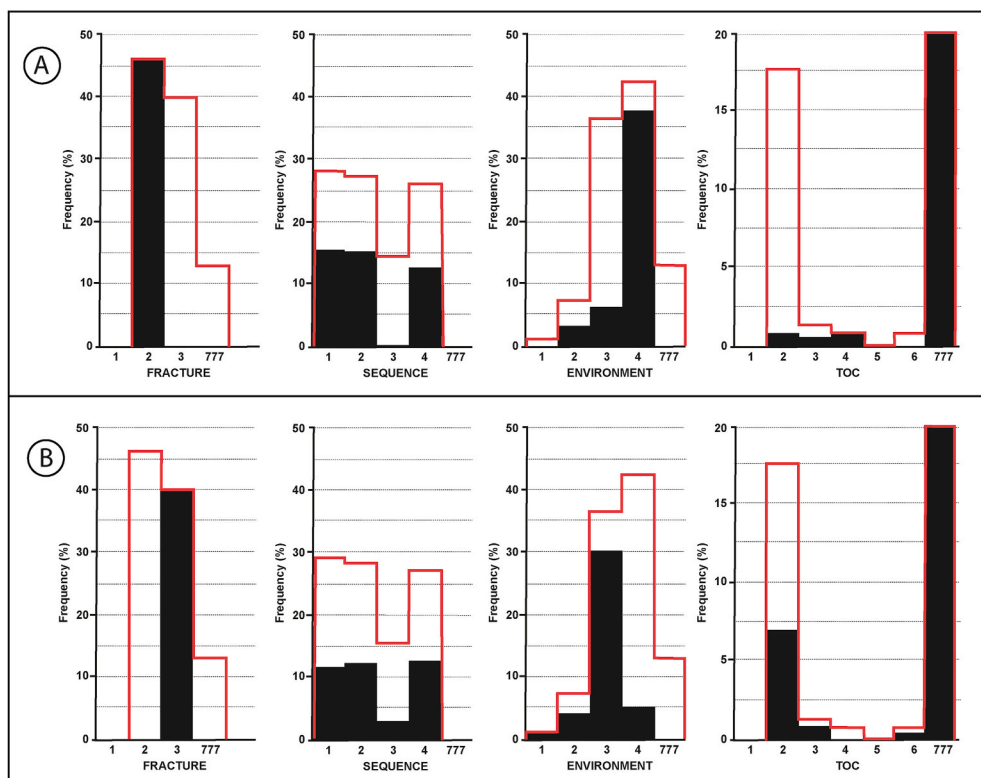


**Fig. 9.** Frequency distribution of the properties FRACTURE, SEQUENCE, ENVIRONMENT and TOC from 16–17 and 12–36 well cores based on the sampled points reported in the spreadsheets of [Tables S3a and S3b](#) (see Supplementary Material). The red line represents the distribution of the whole sampled points where fractures occur (i.e. only the points with codes 2 and 3 of the property FRACTURE). The black bars in the upper (A) and lower (B) histograms represent the sampled points corresponding respectively to the occurrence of the horizontal and vertical to high angle fractures. The “777” values are attributed to cells of the spreadsheets where information on a given property was not available. In the histograms to the right (property TOC) the “777” sampled points represent ~80% of the total. See [Table 1](#) for code explanation. (For interpretation of the references to color in this figure legend, the reader is referred to the Web version of this article.)

the sampled points corresponding to fracture occurrence. The values reported as “777” correspond to undefined, though not null, values that were indeed attributed to cells of the log spreadsheets when information on a given property was not available. This is because at the same well depth information may not be available for all properties (see [Table S3a](#) and [Table S3b](#) of the Supplementary Material).

[Fig. 9A](#) indicates that the horizontal fractures (code 2 of the property FRACTURE) are similarly abundant in 3 of the 4 stratigraphic sequences (property SEQUENCE) and are rare only in sequence 3. They occur in nearly all facies associations (property FACIES). In particular, the massive siltstones (code 6) host 28% of the fractures, whereas the bioclastic siltstones (code 8) and the silt-dominated alternation (code 5) host respectively 7 and 5% of the fractures. Globally, the depositional environment (property ENVIRONMENT) named offshore (code 4) hosts the majority of horizontal fractures. No relationship between the abundance of the horizontal fractures and the host-rock TOC could be highlighted.

[Fig. 9B](#) indicates that the vertical to high angle fractures (code 3 of the property FRACTURE) are similarly abundant in 3 of the 4 stratigraphic sequences (property SEQUENCE) and are fairly less represented in sequence 3. They occur in almost all facies associations (property FACIES). In particular, the sand-dominated alternation (code 4) hosts 29% of the fractures, whereas the massive fine-grained sandstones (code 2) and the bioclastic siltstones (code 8) host respectively 4 and 3% of the fractures. Globally, the depositional environment (property ENVIRONMENT) named offshore transition (code 3), characterized by sand-rich facies, hosts the majority of the vertical fractures. These fractures seem to occur mainly in rocks with low TOC, i.e. between 1 and 2% (code 2 of the property TOC).

#### 4.5. Vein petrography

All the investigated mineralized fractures (i.e. horizontal and vertical to high angle veins) are fully sealed by calcite cements, leaving no fracture porosity left. Despite the monotonous mineralogy, the calcite

cements display various crystalline habitus (e.g. fibrous, blocky and elongated blocky) and spatial arrangement (i.e. texture) within the veins. Details on the petrographic features of all the studied samples (including the fractures and the sealing calcite cements) can be found in [Table S1a](#) and [Table S1b](#) (see Supplementary Material).

The horizontal, bedding-parallel veins are sealed by fibrous, blocky or elongated blocky crystals ([Fig. 10](#)). Commonly, different crystal habitus may occur in the same vein, where for instance the crystals evolve from the vein wall to the vein center from fibrous to elongated blocky or from elongated blocky to blocky. In all these cases, the crystals have syntaxial (both symmetrical or asymmetrical) or antitaxial arrangements suggesting that calcite precipitation occurred during fracture opening (syn-kinematic calcite). Features suggesting a crack-seal mechanism for vein opening are common; we could observe several bands of calcite oriented parallel to the vein walls which represent repeated opening events progressively sealed by calcite ([Ramsay, 1980](#); [Laubach, 2003](#)). The calcite cement may therefore be considered as syn-kinematic, since crack-seal textures form as cement precipitates during progressive vein widening. Our observations also suggest that in most cases, the horizontal veins opened in mode I, even though we could observe in very few cases evidence (slickensides) for mixed mode I-mode II opening ([Fig. 10C](#) and D).

All the vertical to high angle fractures are sealed by blocky to elongated blocky calcite crystals ([Fig. 10](#)). In the first case a drusy texture may be observed with the crystal size increasing towards the vein center, whereas in the second case the crystals have a syntaxial arrangement (both symmetrical and asymmetrical). Features corresponding to crack-seal mechanism of vein opening have been only locally observed. More commonly the vein terminations display tortuous forms, with axial planes lying broadly in the plane of bedding. In most cases also the vertical veins opened in mode I ([Fig. 10A](#) and B).

All the veins show twinned calcite crystals ([Fig. 10](#)). Most twins are thin (thickness < 5  $\mu\text{m}$ ) and rectilinear, suggesting low strain (a few percent) and deformation at temperature below 170–200  $^{\circ}\text{C}$  ([Ferrill et al., 2004](#); [Lacombe, 2010](#)).

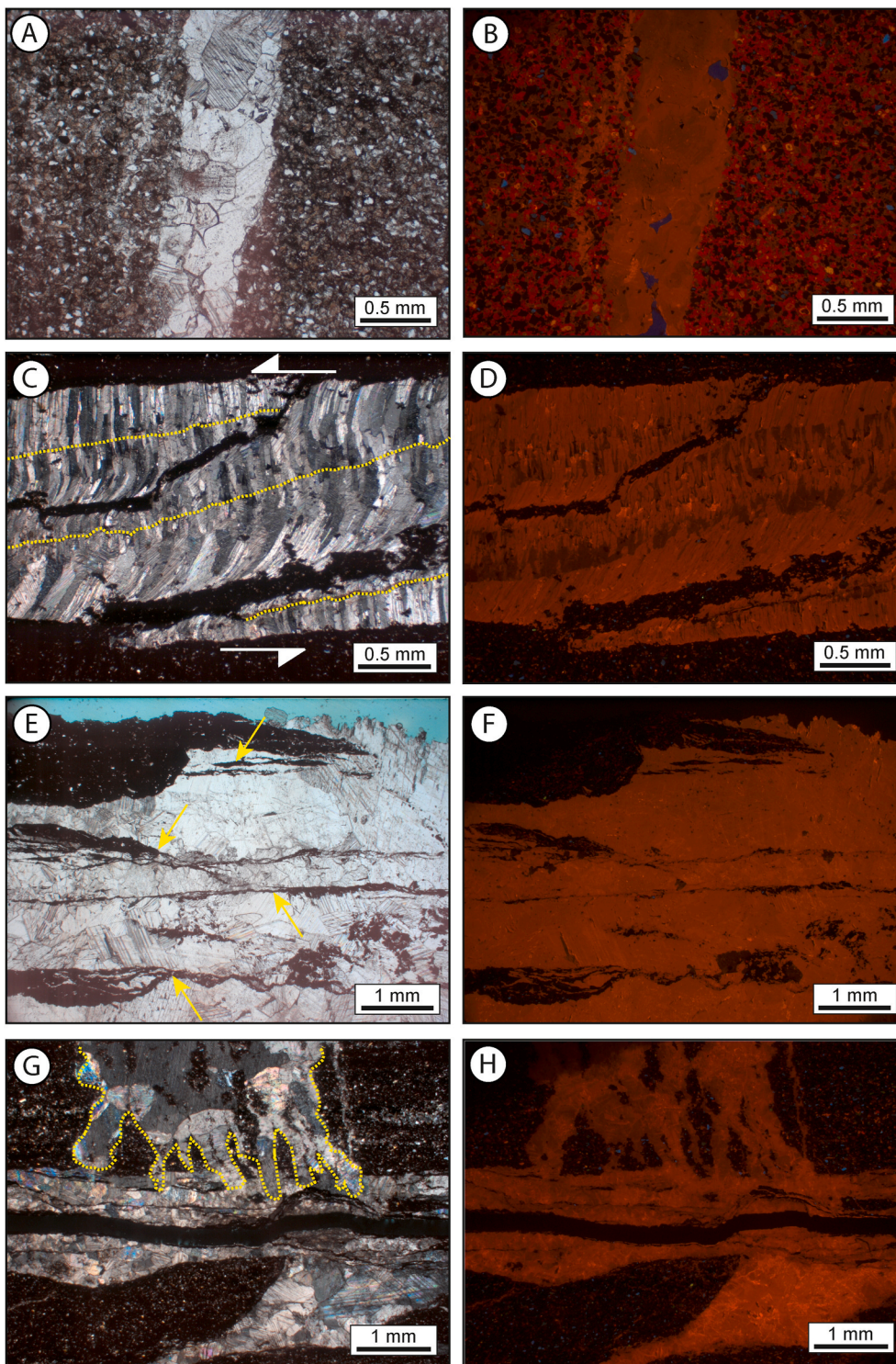


**Fig. 10.** Photomicrographs of cemented fractures (i.e. veins) from the 16–17 and 12–36 wells. All images are oriented with the upper part of the photos corresponding to the stratigraphic up direction. PPL = plane polarized light, CPL = crossed-polarized light, CL = cathodoluminescence. **A.** Vertical vein filled by blocky calcite crystals (sample 16-17-23). PPL. **B.** Same image of A. under CL. The blocky calcite shows uniform, bright orange luminescence. **C.** Horizontal vein filled by fibrous to elongated blocky calcite crystals with antitaxial arrangement. Median planes are highlighted by yellow dotted lines. Crystal deformation suggests mixed mode I-mode II vein opening (sample 12-36-C3-2). CPL. **D.** Same image of C. under CL. The crystals have dominantly bright orange luminescence. Some of them may evolve from bright to dull orange during growth. **E.** Horizontal vein filled by elongated blocky to blocky calcite crystals displaying incremental growth by crack-seal episodes, highlighted (yellow arrows) by strings of wall rock inclusions, demonstrating mode I vein opening (sample 16-17-2). PPL. **F.** Same image of E. under CL. The crystals show uniform bright orange luminescence. **G.** Vertical vein filled by blocky calcite crystals replacing blocky (locally elongated blocky) calcite crystals filling an horizontal vein as highlighted by the yellow dotted line (sample 12-36-C2-2 B). CPL. **H.** Same image of G. under CL. The calcite crystals filling the different veins show undistinguishable uniform bright orange luminescence. (For interpretation of the references to color in this figure legend, the reader is referred to the Web version of this article.)

Interestingly, all calcite cements sealing the fractures, irrespective of the well core of belonging, fracture orientation and crystal habitus/texture, display, when observed under UV-light, the same response given by uniform and very dull green fluorescence. Similarly, the calcite cements cannot be distinguished when observed under CL as they all show a relatively uniform bright orange luminescence.

Cross-cutting and abutting relationships between horizontal and vertical to high angle veins were only locally observed, therefore the vein relative chronology is not easily assessed from petrography only. However, where cross-cutting relationships are observed, they indicate

that some of the vertical veins post-date the horizontal ones since the calcite crystals of the vertical vein replace the calcite crystals of the horizontal one at the vein intersection (Fig. 10G and H).

#### 4.6. O–C–Sr isotope geochemistry

The results of the O–C stable isotope analyses performed on the vein calcite cements are reported in Fig. 11. The  $\delta^{18}\text{O}$  ranges between  $-8.27$  and  $-11.18\text{‰}$  (mean  $-10.45\text{‰}$ ), whereas  $\delta^{13}\text{C}$  ranges from  $1.34$  to  $-4.38\text{‰}$  (mean  $-1.09\text{‰}$ ). When separating the calcite samples per well

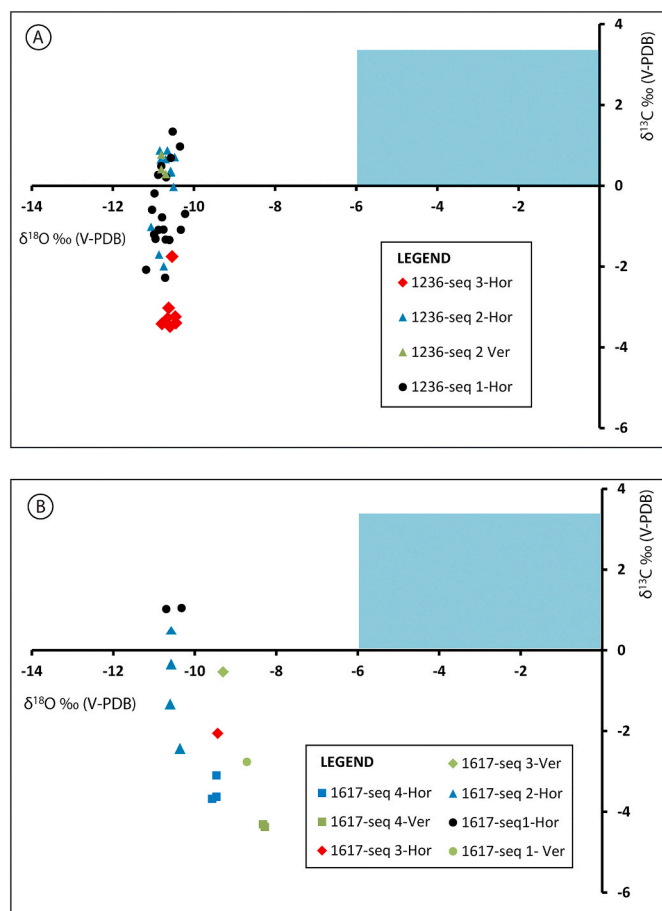


**Fig. 11.** O–C stable isotope composition of the fracture sealing calcite cements. The vein orientation (horizontal or vertical to high angle) and the stratigraphic sequence of belonging are reported. The O–C isotope composition of calcites precipitated in equilibrium from Early to Middle Triassic seawater (from Veizer et al., 1999) is represented by the light blue squares. **A.** Calcite veins from well 16–17. **B.** Calcite veins from well 12–36. (For interpretation of the references to color in this figure legend, the reader is referred to the Web version of this article.)

of belonging it comes that calcite from well 16–17 has  $\delta^{18}\text{O}$  ranging from  $-8.27$  to  $-10.7\%$  (mean  $-9.69\%$ ) and  $\delta^{13}\text{C}$  ranging from  $1.04$  to  $-4.3\%$  (mean  $-1.86\%$ ), whereas calcite from well 12–36 has  $\delta^{18}\text{O}$  varying from  $-10.72$  to  $-11.18\%$  (mean  $-10.72\%$ ) and  $\delta^{13}\text{C}$  varying from  $1.34$  to  $-3.43$  (mean  $-0.82\%$ ).

Analyzed calcites display a very negative  $\delta^{18}\text{O}$  compared to calcite precipitated in equilibrium with Early to Middle Triassic seawater (Fig. 11; Veizer et al., 1999). Based on the well-established dependency of O isotope fractionation on temperature (O'Neil, 1969), such negative  $\delta^{18}\text{O}$  values suggest calcite precipitation at burial temperatures.

The slight  $\delta^{13}\text{C}$  variability of the calcites from the two wells encompasses a comparable range ( $\sim 4\%$ ) and may be due to the contribution of different amounts of light  $^{12}\text{C}$  from the host-rocks to the calcite parent fluids. Indeed, in well 12–36, the most negative  $\delta^{13}\text{C}$  values are recorded by calcites hosted in sequence 3 (Fig. 11A), which is characterized by the highest mean TOC among the three sequences recorded in this well (Table 2). Similarly, in well 16–17, the most negative  $\delta^{13}\text{C}$  values are recorded in samples from sequence 4 (Fig. 11B), which records the highest TOC values of the whole dataset analyzed (Table 2).

Calcites from different well cores and differently oriented veins have overlapping Sr isotope composition (Table S1a and Table S1b of Supplementary Material). Indeed, 10 of the 11 calcites investigated display  $^{87}\text{Sr}/^{86}\text{Sr}$  falling in the narrow range comprised between  $0.7112$  and  $0.7124$ , with only one calcite having lower values ( $0.7091$ ). Compared

with calcites precipitated in equilibrium with Early to Middle Triassic seawater, which have  $^{87}\text{Sr}/^{86}\text{Sr}$  in the range  $0.706940$ – $0.708219$  (Veizer et al., 1999), all of the fracture calcites investigated result to be enriched in the radiogenic  $^{87}\text{Sr}$  isotope.

Overall, these results indicate that the investigated calcites show little variations in isotope compositions irrespective from crystal habitus and texture, vein orientation and well of belonging.

#### 4.7. Fluid inclusion (FI) study

Of the 7 samples prepared for Fluid Inclusion (FI) study only 4 could be investigated for microthermometry. This is because the three other samples consist of fractures sealed by fibrous calcite crystals for which microthermometry measurements were unfeasible due to the small size of the FIs. Four different types of FIs (Type I, Type II, Type III, Type IV) were distinguished petrographically and may show shapes like negative crystals or controlled by crystallographic planes (Fig. 12 and Table 3). The main results of FIs microthermometry are reported in Table 3 and Fig. 13.

Type I consists of aqueous, bi-phase, liquid-rich FIs with degree of fill (F) between  $0.89$  and  $0.95$ ; they occur in crystal cores, along trails or isolated and do not show fluorescence under UV-light (Fig. 12A and B). Homogenization occurs in the liquid state at temperatures (Th) between  $78$  and  $118$  °C with mode value at  $100$  °C. During cooling after homogenization most FIs develop a gas bubble at temperatures between  $88$  and  $62$  °C. During further cooling they freeze at temperatures between  $-67$  and  $-70$  °C. During reheating after freezing, on some FIs ( $n = 15$ ) the occurrence of a first liquid (i.e. the apparent eutectic, which overestimates the real eutectic) was observed optically at temperatures between  $-21.9$  and  $-18.4$  °C, suggesting that the aqueous fluid is dominated by NaCl. Ice is possibly the last phase to melt (as deduced from the roundish shape and the whitish color of the crystals) with a stable behavior (gradual melting allowing cycling procedure). Final melting of ice (Tmi) occurs between  $-19.3$  and  $-16.0$  °C. Fluid salinity, calculated on 15 FIs, varies between  $19.4$  and  $21.9$  eq. NaCl wt% (mode is 20). The salinity of Type I FIs is about six times higher than normal seawater, suggesting that the calcites precipitated from basinal brines. The Th measured represent FI minimum trapping temperatures. To estimate the real trapping temperatures an isochore was constructed using the mode values of Th ( $100$  °C) and salinity (20 eq. NaCl wt%) and combined with a geothermal gradient of  $30$  °C/km. This gradient is consistent with the basin evolution during Mesozoic times, as deduced from the available TemisFlow™ model. A pressure correction of  $10$  °C was evaluated for Type I FIs pointing to a possible trapping temperature of  $110$  °C.

Type II is made of oil, bi-phase, liquid-rich FIs with F between  $0.8$  and  $0.92$ ; they occur in crystal cores, along trails or isolated and show a green fluorescence under UV-light (Fig. 12C and D). Homogenization in the liquid state occurs at temperatures (Th) falling within the  $24$ – $58$  °C range with mode value of  $31$  °C. During cooling after homogenization all FIs develop a gas bubble between  $48$  and  $26$  °C. During cooling runs no solid phases are observed to form.

Type III consists of oil, mono-phase FIs with  $F = 1$ ; they occur in crystal cores, isolated, along growth zones, along trails and show a green fluorescence under UV-light. No phase changes are observed during heating and cooling runs and the FIs remain monophasic. No microthermometry measurements could be performed.

Type IV comprises mono-phase, liquid FIs with  $F = 1$ ; they occur in crystal cores, along growth zones, isolated or along trails. They consistently show shapes from negative crystal to crystallographic controlled. Some of them display weak yellow to green fluorescence whereas some others do not show any fluorescence under UV-light (Fig. 12E and F). During cooling from room temperature, the mono-phase liquid FIs develop a gas bubble at temperatures between  $-60$  and  $-74$  °C. The FIs persist in the bi-phase state down to  $-150$  °C with no observable solid phase being formed. During reheating the bi-phase FIs homogenize in

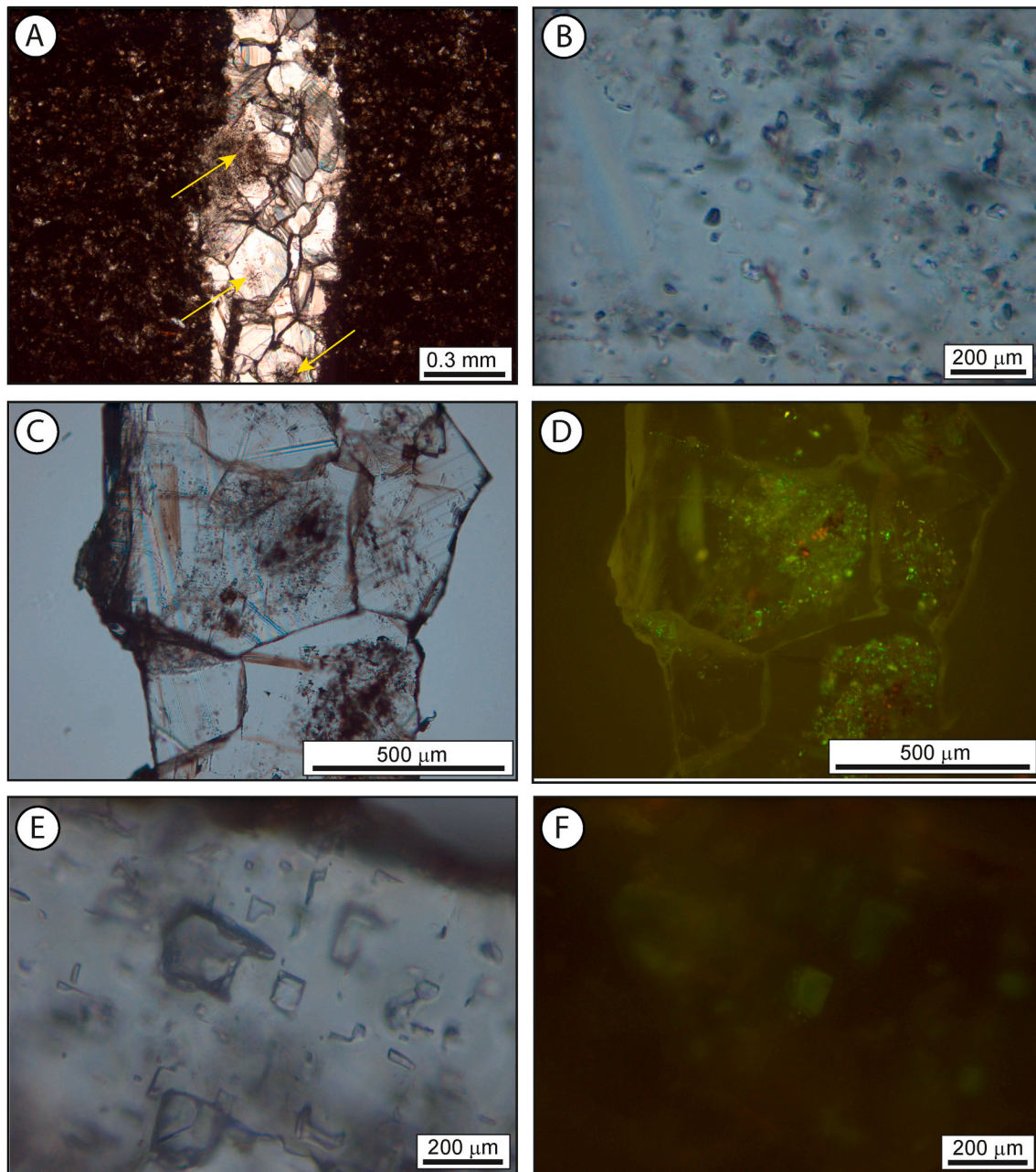


**Fig. 12.** Photomicrographs illustrating some petrographic features of the analyzed FIs at room temperature. **A.** Assemblages of possibly primary Type I FIs (yellow arrows) occurring in the core of calcite crystals (vertical vein, sample 16-17-23). **B.** Details of assemblage of Type I FIs from the same sample illustrated in A. **C.** Assemblage of possibly primary Type II FIs occurring in the calcite crystal cores (vertical vein, sample 16-17-23). **D.** Same image of C. under UV-light revealing a bright green fluorescence for the Type II FIs. **E.** Assemblage of possibly primary Type IV FIs displaying shapes from negative crystal to crystallographically controlled (horizontal vein, sample 12-36-C2-2 B). **F.** Same image of E. under UV-light revealing a weak green fluorescence for some of the Type IV FIs. (For interpretation of the references to color in this figure legend, the reader is referred to the Web version of this article.)

**Table 3**  
Results of FI study from wells 12–36 and 16–17. Sample name, fracture orientation, crystal habitus of the sealing calcite phases, type and petrographic occurrence of fluid inclusions (FI), type of fluid phases and their response under UV-light are reported, together with the range and mode values of homogenization temperatures (Th), ice melting temperatures (Tmi) and calculated salinity. F = degree of fill, C = crystal cores, T = pseudo-secondary trails, I = isolated, Z = growth zones, L = liquid, V = vapor, O = oil, G = gas.

Sample	Vein orientation	Mineral phase/habitus	FI type	Occurrence	Fluid Phases	F	UV-light response		Th (°C)		Tmi (°C)		Salinity (eq. NaCl wt%)	
							response	range	mode (n)	range	mode (n)	range	mode (n)	
1617-23	vertical	calcite/blocky	I	C/T/I	L + V	0.89–0.95	none	78.0/118.0	101 (50)	–16.0/–19.3	–16.5 (15)	19.4/21.9	19.8 (15)	
1617-23	vertical	calcite/blocky	II	C/I	O + G	0.85/0.90	green	36.5/45.0	41.5 (13)	–	–	–	–	
1617-23	vertical	calcite/blocky	III	T	O	1	green	–	–	–	–	–	–	
1617-12	horizontal	calcite/blocky	III	C/I/T	O	1	green	–	–	–	–	–	–	
1617-12	horizontal	calcite/blocky	IV	C/T	L (CH <sub>4</sub> ±CO <sub>2</sub> )	1	yellow/green/none	–	–	–	–	–	–	
C2-1236-2 B	horizontal	calcite/elongated blocky	IV	C/I	L (CH <sub>4</sub> ±CO <sub>2</sub> )	1	yellow/green/none	–69.0/–76.0	–70 (10)	–	–	–	–	
C2-1236-2 B	horizontal	calcite/blocky	III	C/T/I	O	1	green	–	–	–	–	–	–	
C2-1236-2 B	vertical	calcite/blocky	III	C/T/I	O	1	green	–	–	–	–	–	–	
C2-1236-2 B	vertical	calcite/blocky	IV	C/T	L (CH <sub>4</sub> ±CO <sub>2</sub> )	1	green/yellow/none	–62.0/–74.0	–69 (8)	–	–	–	–	
C1-1236-4	horizontal	calcite/elongated blocky	II	Z/C	O	0.80/0.92	green	24.0/58.0	31 (39)	–	–	–	–	
C1-1236-4	horizontal	calcite/elongated blocky	IV	Z/C	L	1	none	–66.0/–71.0	–70 (9)	–	–	–	–	

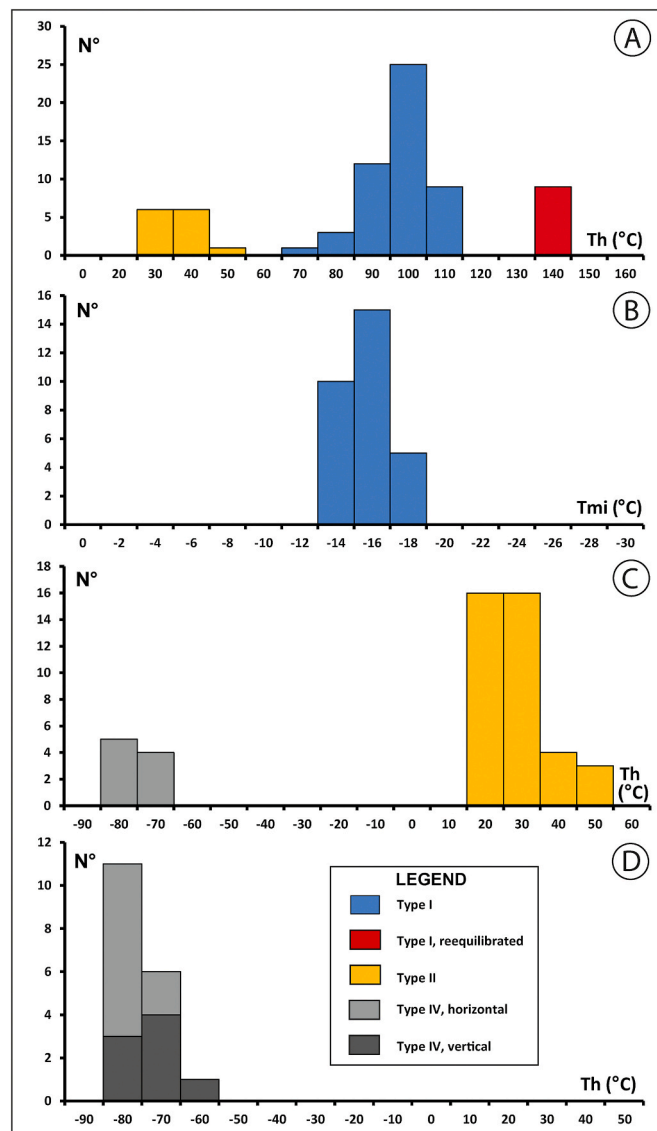


**Fig. 13.** Results of microthermometry for primary FIs in calcite cements from differently oriented veins. A. Frequency distribution of Th values for Type I and Type II FIs (sample 16-17-23, vertical vein). The red bar refers to possibly reequilibrated Type I FIs. B. Frequency distribution of Tmi values for Type I FIs (sample 16-17-23, vertical vein). C. Frequency distribution of Th values for Type IV FIs (sample 12-36-C2-2 B, horizontal and vertical veins). D. Frequency distribution of Th values for Type II and Type IV FIs (sample 12-36-C1-4, horizontal vein). Light and dark grey bars refer to horizontal and vertical veins respectively. (For interpretation of the references to color in this figure legend, the reader is referred to the Web version of this article.)

the liquid state. Homogenization temperatures (Th) are comprised between –76 and –62 °C with mode value at –70 °C. The behavior of Type IV FIs suggests they may be carbonic FIs, belonging to the CH<sub>4</sub>–CO<sub>2</sub>–N<sub>2</sub> fluid system. The behavior of these fluids depends on their density and on the relative proportions of the different components (Van den Kerkhof and Thiery, 2001; Conliffe et al., 2017). In particular, for a pure CH<sub>4</sub> system, Th values of –80 °C are expected with Th becoming less negative with increasing proportions of CO<sub>2</sub>. Th values measured for Type IV FIs (Table 3) are in line with a system dominated by CH<sub>4</sub> with some quantities of CO<sub>2</sub>, although the presence of other hydrocarbons, such as C<sub>2</sub>H<sub>6</sub> or C<sub>3</sub>H<sub>8</sub>, cannot be excluded. Preliminary characterization of Type IV FIs with Raman spectroscopy also revealed the presence of CH<sub>4</sub>, though the high fluorescence of the host calcite mineral did not allow a more quantitative evaluation.

## 5. Discussion

### 5.1. Host-rock controls on fracture occurrence

A number of papers have addressed the multiple factors controlling the occurrence of fractures in siliciclastic tight reservoir rocks (Engelder and Peacock, 2001; Rijken and Cooke, 2001; Peacock and Mann, 2005; Wang and Gale, 2009; Gale et al., 2014; Wang et al., 2016; Ilgen et al., 2017; Hooker et al., 2020; Peng et al., 2020). Many factors related to host-rock properties, such as lithology, bed thickness, abundance of organic matter, mineralogy and cementation have been recognized as potentially exerting a control on the brittleness of the rock (i.e. the easiness of a rock to be fractured and its ability to maintain a fracture).

Rock brittleness is a key criterion to identify the most suitable stratigraphic intervals for hydraulic fracturing and hence, for successful development of unconventional tight oil and gas plays hosted in fine siliciclastic rocks such as the shales and the siltstones. Present day brittleness can be evaluated based on either lithology or elastic properties. In general, the higher the Young's modulus and the lower the Poisson's ratio, the more brittle the rock. For instance, rock mechanical tests indicate that under the same stress conditions, a shale will have higher brittleness and smaller tensile strength if it has lower Poisson's ratio and higher Young's modulus (Ding et al., 2012).

The composition of the shale exerts a first-order control on brittleness, and therefore on fracture system development, both natural and stimulated. The content in relatively hard minerals such as quartz, feldspar and carbonates has been found to be positively correlated with the number of fractures and/or brittleness of the shale (Perez and Marfurt, 2013; Zeng et al., 2013; Labani and Rezaee, 2015; Rybacki et al., 2015, 2016; Wang et al., 2017). Conversely, a high clay content makes the shale more ductile (Aoudia et al., 2010; Perez and Marfurt, 2013; Dong et al., 2017, 2018). The brittleness of a shale can therefore be predicted from the volumetric fraction of clay, quartz, feldspar and carbonate contents by treating the rock as a composite material and by calculating its elastic properties by the rule of mixture (Pei et al., 2016), though this approach does not take into account the effect due to the shape of grains (Peng et al., 2020). The influence of TOC and organic maturity on brittleness of tight siliciclastic rocks is still debated. In the Nunitang Shale the TOC shows a positive correlation with the number of fractures (Zeng et al., 2013). In the Barnett Shale, Perez and Marfurt (2013) show that contrary to the commonly held understanding, the increased TOC does not make the rock more ductile, whereas Yasin et al. (2017) report that the TOC content has a positive correlation with the amount of quartz, and that organic maturity has a positive correlation with brittleness. Dong et al. (2018) also conclude that in the Duvernay shale, increased organic maturity results in greater hardness for rocks of similar geochemical compositions. Conversely, other studies suggest that the effect of organic matter content and maturity on the mechanical properties of a shale is subordinate to the rock mineral composition (Aoudia et al., 2010; Labani and Rezaee, 2015).

In contrast with the well documented literature on shales, the relationship between composition and mechanical properties in siltstones is not well established. In particular, brittleness of the Montney siltstones has been calculated from well-log averages (sonic, density, XRF, XRD) calibrated to static and measured data on cores (Vaisblat et al. 2017a, 2019; Chatellier et al., 2018).

The results of the present study derived from the analysis of cored intervals of wells 12–36 and 16–17 which dominantly correspond to the Montney Fm and to a minor extent to the Doig Fm (Fig. 3), allow considering the succession investigated as being mostly composed by siltstones. According to the frequency distribution analysis accomplished (Fig. 9), based on a rather continuous sampling of the different properties (i.e. SEQUENCE, FACIES, ENVIRONMENT, FRACTURE, TOC) along the logs of the two well cores it could be concluded that:

- The depositional environment named offshore transition (and including facies associations such as sand-dominated alternation and silt-dominated alternation), chiefly composed by coarse silt and fine sand, hosts the majority of the vertical to high angle fractures. These rocks display low to moderate TOC (i.e. between 1 and 2%).
- The depositional environment named offshore (and including facies associations such as massive siltstones, organic-rich siltstones, bioclastic siltstones, laminated siltstones), chiefly composed by fine silt (locally with clay), hosts the majority of horizontal fractures. No relationship between the abundance of the horizontal fractures and the host-rock TOC has been identified.

On the other hand, the petrographic analysis accomplished under CL, based on local observations (i.e. where thin sections were made; see list in Table S1a and Table S1b of the Supplementary Material) from the two investigated wells, suggests that the abundance of diagenetic carbonates (early or late diagenetic; Figs. 6 and 7) does not seem to be a main factor controlling the fracture occurrence, since most of the fracture host-rocks observed in thin section do not contain abundant diagenetic carbonates. An exception is represented by the offshore samples which seem to develop vertical fractures where abundant burial dolomite (D3) occurs.

A further aspect that can be deduced from the results of the present study on wells 16–17 and 12–36 (Fig. 3) is that the vertical facies changes of the studied lithologies (stacking pattern) seem to also influence the horizontal fracture occurrence: the higher the vertical facies heterogeneity, the more numerous the horizontal fractures. This interpretation is supported by the presence of slickenlides locally observed in this study and also described in the Altares Member of the Montney Formation, 10 km NW of the study area (Sanders et al., 2018).

According to these general results issued from the two studied wells it could thus be concluded that fracture occurrence in the Montney siltstones seems to be chiefly controlled by host-rock facies (coarseness) and vertical facies changes (stacking pattern) and to a minor extent by the abundance of diagenetic dolomite. Conversely, host-rock TOC seems not to be correlated with the fracture abundance.

In order to further characterize the factors controlling fracture occurrence in the studied lithologies, these general results issued from the study of the two wells were integrated with available data from well 12–36 on bulk brittleness (computed from XRD and XRF continuous logs and calibrated with core measurements; Chatellier et al., 2018) and mineralogy (British Columbia Oil and Gas Commission public database). Mineralogy is however only available for two of the three investigated cores (i.e. core 1 and core 3; Fig. 14). In spite of the unfortunate lack of mineralogy analysis for core 2 that shows the highest bulk brittleness, the comparison between mineralogy and bulk brittleness of cores 1 and 3 (Fig. 14) suggests that clays/mica content is negatively correlated with brittleness and stiffness. This comparison further shows (Fig. 14) that the calcite/dolomite and K-feldspar/plagioclase contents of core 1 is higher than in core 3, suggesting that these minerals may also control the bulk brittleness. Following Pei et al. (2014), it could be concluded that similarly to shales, the content in relatively hard minerals like feldspars and carbonates may enhance the brittleness of siltstones.

By combining the data on bulk brittleness for well 12–36 (Chatellier et al., 2018) with the occurrence/orientation of fractures (this study) it appears that the relationship between bulk brittleness and fracture occurrence is not straightforward (Fig. 14), so that fracture occurrence cannot be simply predicted from bulk brittleness derived from compositional logs only. Indeed, bedding-parallel horizontal fractures are observed in all of the three cores of well 12–36 despite the strong difference in bulk brittleness. This rather argues in favor of a control being also exerted by mechanical layering. Indeed, in contrast to core 1 which displays more homogeneous sedimentary facies and bulk brittleness, cores 2 and 3 include a number of facies and depositional environments and exhibit high frequency vertical changes in brittleness (Fig. 14). This results in horizontal fractures being less abundant in core 1 than in cores 2 and 3 and conclusively suggests that the occurrence of horizontal



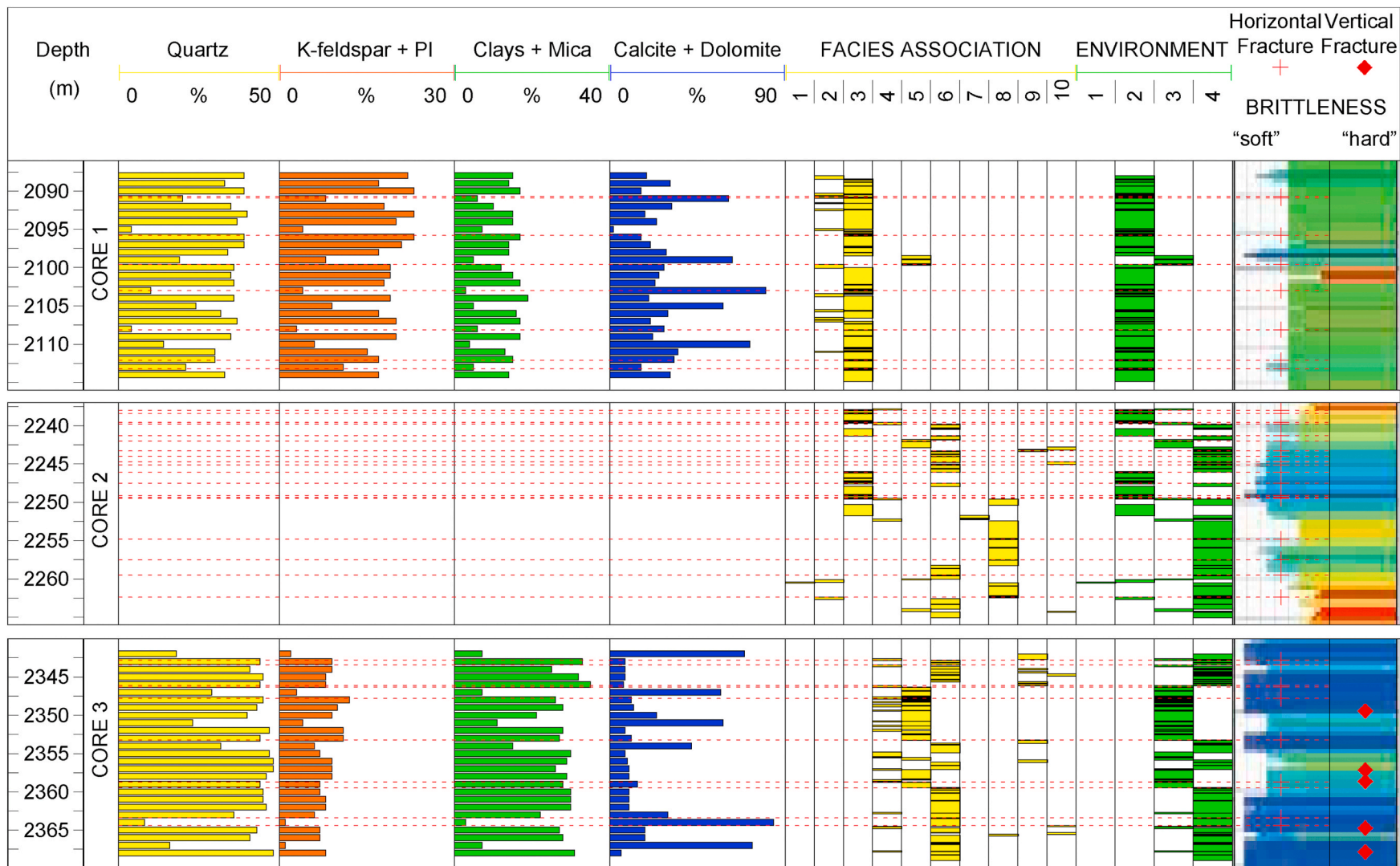


**Fig. 14.** Results of this study (facies associations, depositional environments, location and orientation of fractures) for the three cores (core 1, core 2, core 3) of well 12-36 are reported together with data from literature: mineralogy (from British Columbia Oil & Gas Commission) and bulk brittleness (from Chatellier et al., 2018). High values of brittleness are in red, low values in blue, intermediate values are in green. Mineralogy data are available for core 1 and core 3 only. Red horizontal lines highlight the horizontal fractures. See Fig. 3 for location of the three cores along well 12-36. (For interpretation of the references to color in this figure legend, the reader is referred to the Web version of this article.)

fractures is mainly related to 1) the occurrence of internal facies laminations and 2) the number of interfaces between layers of different brittleness (i.e. sedimentary facies transitions). Therefore, the Montney siltstones like shales seem to exhibit a rather high strength anisotropy (weakness parallel to bedding), though they are stiffer and more brittle than common shales.

Concerning the vertical fractures of well 12–36 (Fig. 14), they mostly occur in core 3 which is composed by facies with the lowest bulk brittleness (likely due to the presence of high clays/mica contents; Fig. 14). This is again hard to explain from the bulk brittleness log only. The results of the present study suggest however that the facies coarseness and/or the presence of D3 ferroan dolomite had a potential role in concentrating these fractures.

Summarizing, our results from wells 16–17 and 12–36 together with the literature data from well 12–36 only (Chatellier et al., 2018, and British Columbia Oil and Gas Commission public database) show that the investigated siltstones have a peculiar mechanical behavior. Indeed, the fracture occurrence seems not to be controlled by the host-rock TOC (Figs. 5 and 9). Furthermore, the lack of direct correlation between the occurrence of fractures and bulk brittleness (calculated according to Chatellier et al., 2018, Fig. 14) suggests that bulk brittleness cannot be used alone as a reliable proxy for predicting the occurrence of natural fractures in such lithologies. Here other factors may play a role, such as the vertical facies heterogeneity and/or the facies coarseness, locally associated with the presence of specific carbonate diagenetic phases.

## 5.2. Fracture timing and foreland evolution

Timing of fracture opening is difficult to constrain, and without this information, ascribing the fractures to a given specific mechanism, is problematic. In the absence of absolute radiometric dating of calcite vein cements (Beaudoin et al., 2018; Hansman et al., 2018; Manganot et al., 2018; Parrish et al., 2018), relative constraints on fracture timing may come from field/core evidence of abutting/crosscutting relationships and petrographic evidence, combined with isotope geochemistry and thermometry evidence (Gabellone et al., 2013; Quesnel et al., 2016; Hooker et al., 2017b, 2019). In particular, the chemical and thermal signatures of the syn-kinematic vein cements reflect fluid conditions during fracturing, and hence may help constraining the timing of fracture opening if combined with thermal basin modeling accounting for the regional tectonic evolution (e.g. Roure et al., 2010; Gasparrini et al., 2014).

In this study, both vertical and horizontal mineralized fractures were investigated from wells 16–17 and 12–36 of the Montney-Doig Fms (Figs. 8 and 10). The strike for the vertical fractures is unknown, which hampers the definition of fracture sets based on their orientation. Therefore, the term “generation” is here used to distinguish calcite veins formed at different times, and possibly by different mechanisms, chiefly based on petrography and FI evidence. Having said this, three generations of veins were identified in the studied wells cores: the first and third oriented vertical to high angle and the second oriented horizontal. Syn-kinematic features like fibrous to elongated blocky calcite crystal habitus arranged in syntaxial to antitaxial textures and/or crack-seal mechanism evidences are common in the three vein generations (see Fig. 10 and Table S1a and Table S1b in the Supplementary Material), allowing to discuss the timing of vein opening from assessing calcite precipitation time.

The three generations of veins are hereafter integrated to the thermal/burial history of the Montney-Doig Fms and interpreted within the geodynamic evolution of the WCSB. (Fig. 15). With such aims, the temperature/depth evolution with time of the Montney-Doig Fms, modeled by the TemisFlow™ software, was used. A 1D thermal curve was extracted for the studied location from the available 3D model (Pauthier et al., 2016), by assuming a thickness of 3300 m of eroded sediments during the Tertiary uplift, according to previous structural restorations (Faure et al., 2004; Hardebol et al., 2009; Roure et al.,

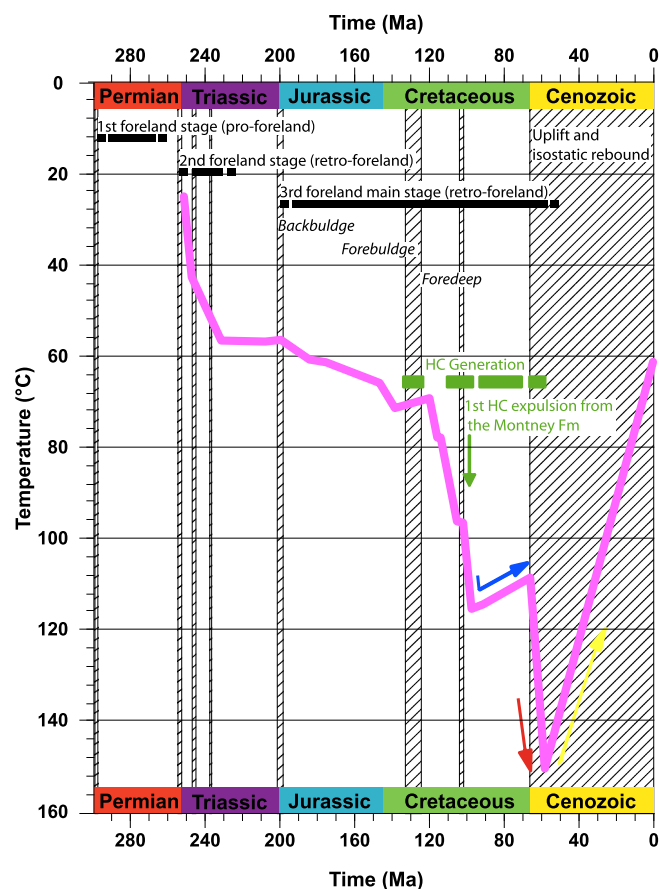


Fig. 15. Thermal evolution of the Montney-Doig Fms, from deposition to present day, modeled with TemisFlow™ by considering 3300 m of eroded sediments during Tertiary uplift (Pauthier et al., 2016; Ducros et al., 2017). The main stages of the basin evolution are reported together with the possible time-temperature frame for the three generations of veins: first vertical generation (blue arrow), second horizontal generation (red arrow), third vertical generation (yellow arrow). (For interpretation of the references to color in this figure legend, the reader is referred to the Web version of this article.)

2010). The curve highlights four main stages in the geological evolution of the WCSB since the Triassic (Fig. 15): 1) a first stage governed by a retro-foreland regime in the Triassic; 2) a transition toward the Jurassic collisional foreland regime; 3) two phases of fast subsidence in the Middle Cretaceous and Latest Cretaceous – Early Paleocene, respectively, separated by a subsidence plateau in the Late Cretaceous; 4) a phase of exhumation and associated sediment erosion or bypass starting from the Early Paleogene, in association with the Laramide Orogeny. The two Cretaceous phases of subsidence and the Early Paleogene exhumation are well time-correlated with the tectonic pulses identified by Pană and van der Pluijm (2015). Notably, the temperatures modeled for the maximum rock burial do not exceed 150 °C (given uncertainties), in agreement with the observation that the calcite crystals from all veins displays thin and rectilinear twins (Fig. 10), suggesting that twinning occurred at temperatures below 170–200 °C (Ferrill et al., 2004; Lacombe, 2010).

The first generation of vertical veins is cemented by calcite precipitated at about 110 °C from basinal brines (20 eq. NaCl wt%) and which also carries oil inclusions (Table 3 and Fig. 13), recording that the oil generation had already started. Triassic source rocks from the WCSB started to generate HC during the Late Cretaceous (88.5 Ma) based on Ducros et al. (2017), and even earlier based on Ness (2001). Accordingly, the age of the first vein generation is bracketed between 100 Ma and 70 Ma, i.e. a time span post-dating the beginning of oil generation and consistent with a 110 °C burial temperature for the studied

succession (Fig. 15). These vertical veins therefore possibly opened during the Late Cretaceous when vertical movements of the foreland were still limited and fast sedimentation of the Colorado Group had occurred (Pană and van der Pluijm, 2015; Ducros et al., 2017; Rohais et al., 2018). Since the strike of these vertical veins is unknown, it is not possible to determine under which stress regime they developed. They could have formed either under a burial/flexure related vertical maximum principal stress  $\sigma_1$  or under a horizontal maximum principal stress  $\sigma_1$  oriented NE-SW that was likely prevailing during the Cretaceous in the Rocky Mountains (Vandeginste et al., 2012) if tectonic stress magnitude had already overcome the burial-related stress magnitude in the basin at that time (e.g. layer-parallel shortening, Tavani et al., 2015).

The horizontal, layer-parallel, veins (second generation) are cemented by calcite which hosts mono-phase liquid  $\text{CH}_4 \pm \text{CO}_2$  inclusions, together with oil inclusions, indicating that they formed after the onset of gas generation. Though the trapping conditions for these HC inclusions could not be estimated, the presence of  $\text{CH}_4$  strongly suggests that the calcite cements precipitated at temperatures higher than 110 °C (i.e. higher than the temperature inferred for the vertical veins of the first generation). Triassic source rocks from WCSB reached the maximum transformation rate just before maximum burial (~58–57 Ma) which also corresponds to a maximum overpressure in these rocks, due to peak HC generation and secondary cracking of oil into gas (Ducros et al., 2017). Therefore, the horizontal veins are interpreted to have formed during Late Cretaceous to Early Paleogene, just before the host lithologies reached the thermal/burial maximum (Fig. 15).

Despite the multiple sources of uncertainties, the age for thermal/burial maximum (~58–57 Ma) is rather close to the age of the last tectonic pulse (~54–52 Ma) identified by Pană and van der Pluijm (2015). The formation of such horizontal, layer-parallel veins at nearly the maximum burial depth was likely associated with pore-fluid pressures exceeding the vertical overburden load (e.g. Price, 1994). The mechanisms for opening horizontal fractures has been recently summarized by Hooker et al. (2019). In case of prevailing strike-slip faulting stress regime, the horizontal fracture opening would have required a poro-elastic effect in response to fluid pressure increase in order to counteract the overburden and the lateral stress in proportion (Engelder and Fischer, 1994), flipping the vertical stress to be the least compressive stress by the time the tensile failure criterion is reached. However, the most likely explanation is that the bedding-parallel veins were related to catagenesis and formed from fluid overpressure within a thrust-faulting regime (in which the overburden is the least compressive stress), in line with the Eocene pulse of regional contraction (Pană and van der Pluijm, 2015) and the compressional or transpressional stress regime reconstructed by Vandeginste et al. (2012) in the Rocky Mountains to the South East. The overpressure increase, here likely induced by  $\text{CH}_4$  generation, is in agreement with earlier works emphasizing the role of HC generation as potential drivers of fracture growth in organic-rich mudrocks (Spencer, 1987; Ozkaya, 1988; Vernik, 1994; Jochum et al., 1995; Marquez and Mountjoy, 1996; Zanella et al., 2014; Meng et al., 2017). Although the horizontal fractures are interpreted to be chiefly governed by gas generation, they are not more abundant in high TOC levels (Fig. 9). This apparent paradox may be explained by the entire succession being overpressured throughout together with the high frequency vertical facies changes of the studied rocks (already underlined in section 5.1). Indeed, these rocks consist of dm to m scale alternations of OM-rich and more arkosic/carbonatic siltstones; it seems likely that peak gas generation provided distributed fluid overpressures that concentrated fracturing in the more brittle beds located above or below the OM-rich ones. Secondary cracking of early migrated oil may also have contributed to the lack of correlation between TOC and fracture occurrence.

Finally, the third generation of vertical veins shows petrographic evidence for post-dating the bedding-parallel ones of second generation (Fig. 10G and H) and also contains monophasic liquid  $\text{CH}_4 \pm \text{CO}_2$

inclusions. We propose that these vertical veins opened during basin uplift (Middle-Late Paleogene) that occurred after peak burial. Vein opening is here interpreted as resulting from the progressive decrease of the far-field horizontal stress magnitude and the transition from Laramide compression to regional transtensional faulting regime (Middle Paleogene). This new tectonic stress was likely combined to residual fluid overpressure to drive the opening of the vertical fractures at depth. The proposed fracture timing is in line with the study of Chatellier et al. (2018) who identified overpressure associated with tectonic uplift by comparing the reservoir pressures against normal hydrostatic pressure trends and also with the model of Ducros et al. (2017) indicating that a fluid overpressure regime persisted after thermal/burial maximum in areas where HC occurred.

In conclusion, the opening of the horizontal veins related to gas generation certainly required fluid overpressure to overcome the weight of the overburden. The occurrence of relatively abundant vertical veins at depth may indicate that their formation was also probably assisted by elevated fluid pressures. In this study however, the quantification of fluid pressure remained out of reach. Only the fine investigation of immiscible co-genetic fluid inclusions (e.g. Roure et al., 2010) or the joint application of thermometric techniques (e.g. Mangenot et al., 2017; Honlet et al., 2018) may potentially give access to fluid pressure conditions during calcite crystal growth and confirm the proposed hypotheses.

### 5.3. Calcite parent fluids and openness of the system

Paleo-water (or paleo-fluid) circulation in sedimentary basins plays a key role in governing burial diagenetic processes (Bjørlykke, 1994; Kyser et al., 2000; Roure et al., 2005). Previous studies have stressed the importance of establishing the origin of burial diagenetic fluids in siliciclastic successions (Morad et al., 2002; Bjørlykke and Jahren 2012; Deschamps et al., 2012). Indeed, aiming to predict the spatial and temporal distribution of diagenetic alterations at basin scale and the present day heterogeneities in the reservoirs, it is of prime importance to define whether reactions were accomplished by fluid advection (active flow) or diffusion (no flow), or in other words whether the fluids were locally sourced (closed system) or derived from external sources (open system). In this respect, the openness of fluid systems driving diagenetic reactions (including carbonate cementations) may be assessed by investigating the occurrence of mineral assemblages and their isotope and elemental geochemistry (Boni et al., 2000; Day-Stirrat et al., 2010; Fantle et al., 2010; Khalifa and Gasparrini, 2014; Swart, 2015). Organic-rich mudrocks represent a peculiar case of siliciclastic rocks, since together with the paleo-waters, they may host locally sourced HC fluids. Here, the investigation of both diagenetic minerals and organic components may help to characterize the openness of the paleo-water and petroleum systems.

The Montney-Doig Fms have been long investigated at the scale of the WCSB to determine the origin of their HC to finally discriminate if they mostly consist in tight reservoirs (where HC migrated from an external source) or if they locally also behaved as source-rocks (where HC are internally sourced). It is commonly accepted that the Doig Fm contains a prolific source rock interval (the Doig Phosphatic Member) and produced liquid HC (Creaney and Allan, 1990; Riediger et al., 1990a; Allan and Creaney, 1991; Ness, 2001; Ejezie, 2007; Ducros et al., 2017). Conversely, despite the Montney Fm contains huge unconventional oil and gas resources, there is less consensus on the potential contribution of the Montney lithologies to the overall produced HC. Indeed, the studies on organic components conducted so far do not find a common agreement and both hypotheses (tight reservoirs *versus* source rocks) are presently supported.

On one side, it is believed that the organic matter from the Montney rocks is composed almost entirely of solid bitumen or pyrobitumen (Chalmers and Bustin, 2012; Sanei et al., 2015; Wood et al., 2015, 2018, 2020; Ardakani et al., 2020a). In particular, a modified Rock-Eval

procedure and organic petrography were applied by Sanei et al. (2015) on Montney Fm samples from one well core located ca. 50 Km South of Fort St. John, within the inherited structure from the PRA collapse (Fig. 1A). Based on the absence of primary deposited kerogen, these authors concluded that the majority of the TOC in the studied samples consists of solid bitumen (or pyrobitumen). The latter resulted from the secondary cracking of a former liquid oil phase which migrated into the larger paleo-intergranular pore spaces of the organically lean rocks of the Montney Fm. Sanei et al. (2015) also believe in previous oil-source rock correlation studies (Riediger et al., 1990a, 1990b) based on biomarker signatures and suggesting that all oils produced from Triassic rocks in the WCSB have been sourced either from the Doig Fm or the Nordegg Member of the Fernie Fm.

On the other hand, a study conducted by Romero-Sarmiento et al. (2016b) on core and cutting samples (partly falling close to wells 16–17 and 12–36) led to the conclusion that the Montney Fm may contain potential source rock beds. Based on artificial thermal maturation, organic petrography and gas chromatography, these authors indicate that the samples represent a series from immature and early mature source rocks with preserved liptinite, to post-peak-mature and over-mature source and tight reservoir rocks containing abundant solid bitumen.

Montney lithologies from cores and cuttings distributed in a large area and encompassing well 16–17, were analyzed by Crombez et al. (2016) for organic content and for major and trace element concentrations. Their results illustrate that sequence 3 presents propitious redox conditions and primary productivity for source rocks development and emphasize the occurrence of primary deposited kerogen in this stratigraphic interval.

The presence of source-rock intervals in the Montney Fm is also supported by Feng et al. (2016, 2017), who identified three different oil families with distinct geochemical signatures within HC accumulations of the Montney Fm. One of the oil family appears to be originated from the Montney Fm since it bears striking resemblance to the corresponding rock extracts.

Finally, very recent studies also highlighted the presence of primary organic facies, coexisting with disseminated and pore-filling solid bitumen in the Montney Fm from Alberta (Ardakani et al., 2020b; Becerra et al., 2020). These observations further call into question the possible local source of the HC within this formation.

The present survey, conducted on mineralized fractures from two wells (16–17 and 12–36) located ca. 70 km North-West of Fort St. John (i.e. in between the HRSZ and the inherited structure from the PRA collapse; Fig. 1A), may bring some light from independent observations to this controversy. In the samples here investigated, three different generations of veins were identified (Fig. 10), carrying different types of HC fluids (Table 3) and having different timing within the WCSB geological and geodynamic evolution (Fig. 15). Many of the studied veins are filled by calcite crystals with fibrous to elongated blocky habitus in syntaxial to antitaxial arrangements and may display features of crack-seal mechanism (Fig. 10 and Tables S1a and S1b from Supplementary Material). This suggests that the mineral precipitation commonly occurred during vein opening (syn-kinematic calcite) so that the fractures were never particularly porous throughout growth. The UV-light and CL response (chiefly governed by Fe and Mn contents), together with the isotope composition, are very similar for all the studied calcite cements, irrespective of the well core of belonging, the vein generation and the crystal habitus/textures (Figs. 10 and 11). In conclusion, despite the different timing of the vein calcites (Late Cretaceous to Paleogene), precipitating at different maturity stages of the HC system, the calcite cements display similar petrographic and geochemical features. This conclusively points at fluids in continuous equilibrium with the host-rocks (Hooker et al., 2017b, 2019). According to this scenario, the calcite veins identified probably formed as hydraulic fractures from a closed fluid system which would have persisted during the burial history of the studied lithologies.

Another argument in favor of this closed-system hypothesis is the lack of diagenetic sulfate minerals within the studied samples (Fig. 7). This contrasts with the occurrence of anhydrite and barite in samples from well cores located South of Fort St. John (within the inherited structure from the PRA collapse; Liseroudi et al., 2020), and which is interpreted as due to the contribution of externally sourced paleo-waters (i.e. sulfate-bearing fluids originated from the dissolution of underlying Devonian evaporites and migrated upwards through deep-seated faults/fractures to the Montney Fm).

The present survey does not question the occurrence of pyrobitumen or of primary kerogen in the Montney-Doig system throughout the WCSB and deciphering between migrated and in place HC in these lithologies at basin scale is far beyond our scopes. Nevertheless, this study clearly suggests that, at least in the limited portion of the basin investigated, the advection of externally sourced paleo-waters (*sensu* McCaig and Knipe, 1990) was not recorded during the precipitation of calcites within the three fracture generations identified (Fig. 15). The lack of evidence for externally sourced paleo-waters is rather in agreement with a local closed-system behavior for the studied rocks, which would thus be in line with the hypothesis of a system that may have self-sourced and retained HC. As the studied wells are located in between the HRSZ and the inherited structure from the PRA collapse (Fig. 1A), we may speculate that this area was primarily characterized by a closed-system hydrodynamic regime, at least during the Late Cretaceous to Paleogene evolution of the basin. This may have important implications for future exploration.

## 6. Conclusions

A multidisciplinary approach (including sedimentology, Rock-Eval pyrolysis, petrography, O–C–Sr isotope geochemistry and fluid inclusion microthermometry) has been applied for the first time to natural mineralized fractures (veins) hosted by mudrocks of the Lower-Middle Triassic Montney-Doig unconventional resource play from the Western Canada Sedimentary Basin.

Montney-Doig well core samples (ca. 2100–2500 m in depth) were collected from two wells in British Columbia. These rocks were deposited in shoreface to offshore environments and display variable mineralogy and organic content (TOC of 0.6–6.6 wt%).

Main analytical results of this survey allow for drawing the following three-fold conclusions:

- 1) Fracture occurrence was chiefly controlled by host-rock facies and only to a minor extent by host-rock diagenesis. Horizontal (bed-parallel) fractures are preferentially localized in very fine facies (siltstones and siltstones with clays) of the offshore environment and where high frequency facies changes induced vertical heterogeneities. Vertical to high angle fractures are more abundant in the coarser facies of the offshore transition environment (coarse siltstones and fine sandstones), though they may also occur in offshore facies (e.g. calcispheric dolosiltstones) which have undergone burial dolomitization. Interestingly, host-rock TOC seems not to have controlled fracture occurrence.
- 2) Three generations of calcite cemented fractures were identified:
  - The first generation (vertical veins), cemented by calcite precipitated at ~110 °C from basinal brines and carrying oil inclusions, records that oil generation had begun; they possibly opened when vertical movements of the foreland were limited and rapid sedimentation of the Colorado Group had occurred (Late Cretaceous).
  - The second generation (horizontal veins), cemented by calcite carrying CH<sub>4</sub>±CO<sub>2</sub> and oil inclusions, originated during peak HC generation; they possibly opened just before maximum burial (Late Cretaceous - Early Paleogene) as a result of overpressures induced by CH<sub>4</sub> generation, assisted by compressive horizontal stress. Fairly distributed fluid overpressures throughout the succession would

explain why they principally developed in the more brittle lithologies, rather than in the OM-rich intervals.

- The third generation (vertical veins), cemented by calcite also containing  $\text{CH}_4 \pm \text{CO}_2$  inclusions, possibly opened during basin uplift (Middle-Late Paleogene) due to horizontal stress decrease, assisted by residual fluid (gas) overpressure.
- 3) UV-light and CL response of the calcite cements together with their isotope geochemistry signature are quite consistent, irrespective of the vein generation and well core of belonging, pointing at lack of evidences for externally sourced paleo-waters. This suggests a closed system behavior for the studied rocks during Late Cretaceous – Paleogene times, at least in the limited portion of the basin investigated.

Overall the study underlines the relevance and usefulness of the applied methodological approach to characterize fracture controls, paleo-fluid circulation and openness of the fluid system in naturally fractured unconventional plays, with implications for exploration.

#### Credit author statement

Marta Gasparrini: Conceptualization, Writing – original draft, Supervision, Investigation, Visualization, Olivier Lacombe: Writing – original draft, Supervision, Sébastien Rohais: Conceptualization, Writing – review & editing, Visualization, Moh Belkacemi: Investigation, Visualization, Tristan Euzen: Writing – review & editing, Resources.

#### Declaration of competing interest

The authors declare that they have no known competing financial interests or personal relationships that could have appeared to influence the work reported in this paper.

#### Acknowledgements

The core-lab of the BC Oil & Gas Commission from Fort St. John is thanked for assistance during core logging and sampling. We are grateful to W. Sassi (head of the “non-conventional gas” project at IFP Energies nouvelles) for funding the whole survey and for scientific advice during its preliminary stages. The ISTeP laboratory (Sorbonne Université) is acknowledged for funding a 5 months internship grant for M. Belkacemi at IFP Energies nouvelles. D. Pillot (IFP Energies nouvelles) helped with the Rock-Eval measurements and interpretation. We acknowledge M. Enter and M. Power from SGS (now at Vidence Inc.), for providing the Qemscan data of well 12–36. Prof. M. Joachimski (GeoZentrum Nordbayern) is thanked for O–C isotope analysis of calcites. The SUERC laboratory is thanked for  $^{87}\text{Sr}/^{86}\text{Sr}$  analysis of calcites. The authors also wish to thank the two reviewers (Kitty L. Milliken and John N. Hooker) for their constructive comments that allowed significant improvement of the manuscript.

#### Appendix A. Supplementary data

Supplementary data to this article can be found online at <https://doi.org/10.1016/j.marpetgeo.2020.104826>.

#### References

- Allan, J., Creaney, S., 1991. Oil families of the western Canada basin. *Bull. Can. Petrol. Geol.* 39 (2), 107–122.
- Aoudia, K., Miskimins, J.L., Harris, N.B., Mnich, C.A., 2010. Statistical analysis of the effects of mineralogy on rock mechanical properties of the Woodford shale and the associated impacts for hydraulic fracture treatment design. In: 44th US Rock Mechanics Symposium and 5th US-Canada Rock Mechanics Symposium. American Rock Mechanics Association.
- Ardakani, O.H., Hlohowskyj, S.R., Chappaz, A., Sanei, H., Liseroudi, M.H., Wood, J.M., 2020a. Molybdenum speciation tracking hydrocarbon migration in fine-grained

- sedimentary rocks. *Geochem. Cosmochim. Acta.* <https://doi.org/10.1016/j.gca.2020.06.006>.
- Ardakani, O.H., Becerra, Daniela, Mackie, S.J., Pedersen, P.K., Reyes, J., Wood, J.M., Sanei, H., Clarkson, C.R., 2020b. Organic Matter in the Alberta Montney Re-visited: Evidence for Primary Organic Matter and Local Hydrocarbon Migration. *Geoconvention, virtual event, September 2020*.
- Armitage, J.H., 1962. Triassic oil and gas occurrences in northeastern British Columbia, Canada. *Bull. Can. Petrol. Geol.* 10 (2), 35–56.
- Bailey, T.R., McArthur, J.M., Prince, H., Thirlwall, M.F., 2000. Dissolution methods for strontium isotope stratigraphy: whole rock analysis. *Chem. Geol.* 167, 313–319. [https://doi.org/10.1016/S0009-2541\(99\)00235-1](https://doi.org/10.1016/S0009-2541(99)00235-1).
- Beaudoin, N., Lacombe, O., Roberts, N.M., Koehn, D., 2018. U-Pb dating of calcite veins reveals complex stress evolution and thrust sequence in the Bighorn Basin, Wyoming, USA. *Geology* 46, 1015–1018.
- Becerra, D., Clarkson, C.R., Ghanizadeh, A., Ardakani, O.H., 2020. First-Time Characterization of Black Shaly Facies along a Full Montney Core: Lithofacies Controls on the Distribution of Primary Organic Matter. *Geoconvention, virtual event, September 2020*.
- Behar, F., Beaumont, V., Penteado, H.L., 2001. Rock-Eval 6 technology: performances and developments. *Oil Gas Sci. Technol.* 56, 111–134. <https://doi.org/10.2516/ogst.2001013>.
- Birck, J.L., 1986. Precision K-Rb-Sr isotopic analysis: application to Rb-Sr chronology. *Chem. Geol.* 56, 73–83. [https://doi.org/10.1016/0009-2541\(86\)90111-7](https://doi.org/10.1016/0009-2541(86)90111-7).
- Bjørlykke, K., 1994. Fluid-flow processes and diagenesis in sedimentary basins. In: Parnell, J. (Ed.), *Geofluids: Origin, Migration and Evolution of Fluids in Sedimentary Basins*, vol. 78. Geological Society, London, Special Publications, pp. 127–140. <https://doi.org/10.1144/GSL.SP.1994.078.01.11>.
- Bjørlykke, K., Jahren, J., 2012. Open closed geochemical systems during diagenesis in sedimentary basins: constraints on mass transfer during diagenesis and the prediction of porosity in sandstone and carbonate reservoirs. *AAPG (Am. Assoc. Pet. Geol.) Bull.* 96 (12), 2193–2214. <https://doi.org/10.1306/04301211139>.
- Bodnar, R.J., 1993. Revised equation and table for determining the freezing point depression of  $\text{H}_2\text{O}$ -NaCl solutions. *Geochem. Cosmochim. Acta* 57 (3), 683–684.
- Boni, M., Iannace, A., Bechstædt, T., Gasparrini, M., 2000. Hydrothermal dolomites in SW Sardinia (Italy) and Cantabria (NW Spain): evidence for late-to post-Variscan widespread fluid-flow events. *Journal of geochemical exploration* 69, 225–229. [https://doi.org/10.1016/S0375-6742\(00\)00020-0](https://doi.org/10.1016/S0375-6742(00)00020-0).
- Bons, P.D., Elburg, M.A., Gomez-Rivas, E., 2012. A review of the formation of tectonic veins and their microstructures. *J. Struct. Geol.* 43, 33–62.
- Chalmers, G.R., Bustin, R.M., 2012. Geological evaluation of Halfway–Doig–Montney hybrid gas shale–tight gas reservoir, northeastern British Columbia. *Mar. Petrol. Geol.* 38, 53–72.
- Chatellier, J.-Y., Simpson, K., Perez, R., Tribovillard, N., 2018. Geochemically focused integrated approach to reveal reservoir characteristics linked to better Montney productivity potential. *Bull. Can. Petrol. Geol.* 66 (2), 516–551.
- Cobbold, P.R., Zanella, A., Rodrigues, N., Løseth, H., 2013. Bedding-parallel fibrous veins (beef and cone-in-cone): worldwide occurrence and possible significance in terms of fluid overpressure, hydrocarbon generation and mineralization. *Mar. Petrol. Geol.* 43, 1–20.
- Conliffe, J., Burden, E.T., Wilton, D.H., 2017. The use of integrated fluid inclusion studies for constraining petroleum charge history at Parsons Pond, Western Newfoundland, Canada. *Minerals* 7 (3), 39.
- Creaney, S., Allan, J., 1990. Hydrocarbon generation and migration in the western Canada sedimentary basin. In: Brooks, J. (Ed.), *Classic Petroleum Provinces*, vol. 50. Geological Society Special Publication, pp. 189–202.
- Crombez, V., 2016. *Petrofacies, Sedimentology and Stratigraphic Architecture of Organic Rich Rocks. Insights from a Multi-Disciplinary Study of the Montney and Doig Formations (Lower and Middle Triassic, Alberta – British Columbia, Canada)*. PhD thesis. VI University, Paris, p. 238. IFPEN report 66669.
- Crombez, V., Baudin, F., Rohais, S., Riquier, L., Euzen, T., Pauthier, S., Ducros, M., Caron, B., Vaisblat, N., 2016. Basin scale distribution of organic matter in marine fine grained sedimentary rocks: insight from sequence stratigraphy and multi-proxies analysis in the Montney and Doig formations. *Mar. Petrol. Geol.* 83, 382–401.
- Crombez, V., Rohais, S., Baudin, F., Euzen, T., Zonneveld, J.-P., Power, M., 2019. 3D stratigraphic architecture, sedimentary budget, and sources of the Lower and Middle Triassic strata of Western Canada: evidence for a major basin structural reorganization”. *Petrol. Geosci.* <https://doi.org/10.1144/petgeo2019-024>.
- Curtis, J.B., 2002. Fractured shale-gas systems. *AAPG (Am. Assoc. Pet. Geol.) Bull.* 86 (11), 1921–1938.
- Davies, G.R., 1997. The Triassic of the Western Canada Sedimentary Basin tectonic and stratigraphic framework, paleogeography, paleoclimate and biota. *Bull. Can. Petrol. Geol.* 45, 434–460.
- Davies, G.R., Moslow, T.F., Sherwin, M.D., 1997. The lower Triassic Montney formation, west-central Alberta. *Bull. Can. Petrol. Geol.* 45 (4), 474–505.
- Davies, G.R., Hume, D., Fox, A., Haysom, S., Nevokshonoff, G., Reinmiller, R., 2014. Core-based structural fabrics in mudstones of the WCSB: ‘PSF’ and cleavage. In: *Unconventional Resources Technology Conference*, August 25–27, Denver, CO, USA.
- Davies, G.R., Watson, N., Moslow, T.F., MacEachern, J.A., 2018. Regional subdivisions, sequences, correlations and facies relationships of the Lower Triassic Montney Formation, west-central Alberta to northeastern British Columbia, Canada — with emphasis on role of paleostructure. In: Euzen, T., Moslow, T.F., Caplan, M. (Eds.), *The Montney Play: Deposition to Development*, vol. 66. *Bulletin of Canadian Petroleum Geology*, pp. 23–92, 1.
- Dawson, M., Kalkreuth, W., 1994. Coal rank and coalbed methane potential of Cretaceous/Tertiary coals in the Canadian Rocky Mountain foothills and adjacent

- foreland: 1. Hinton and Grande Cache areas, Alberta. *Bull. Can. Petrol. Geol.* 42 (4), 544–561.
- Day-Stirrat, R.J., Milliken, K.L., Dutton, S.P., Loucks, R.G., Hillier, S., Aplin, A.C., Schleicher, A.M., 2010. Open-system chemical behavior in deep wilcox group mudstones, Texas Gulf Coast, USA. *Mar. Petrol. Geol.* 27, 1804–1818.
- DeCelles, P.G., 2004. Late Jurassic to Eocene evolution of the Cordilleran thrust belt and foreland basin system, western USA. *Am. J. Sci.* 304, 105–168. <https://doi.org/10.2475/ajs.304.2.105>.
- Deschamps, R., Kohler, E., Gasparrini, M., Durand, O., Euzen, T., Nader, F.H., 2012. Impact of mineralogy and diagenesis on reservoir quality of the lower Cretaceous upper manville formation (Alberta, Canada). *Oil Gas Sci. Technol.* 67 (1), 31–58. <https://doi.org/10.2516/ogst/2011153>.
- Dewhurst, D.N., Yang, Y., Aplin, A.C., 1999. Permeability and Fluid Flow in Natural Mudstones, vol. 158. Geological Society, London, Special Publications, pp. 23–43.
- Dickson, J.A.D., 1966. Carbonate identification and genesis as revealed by staining. *J. Sediment. Res.* 36 (2), 491–505.
- Ding, W., Li, C., Li, C., Xu, C., Jiu, K., Zeng, W., Wu, L., 2012. Fracture development in shale and its relationship to gas accumulation. *Geoscience Frontiers* 3 (1), 97–105.
- Dixon, J., 2000. Regional lithostratigraphic units in the triassic Montney formation of western Canada. *Bull. Can. Petrol. Geol.* 48, 80–83.
- Dong, T., Harris, N.B., Ayranci, K., Yang, S., 2017. The impact of rock composition on geomechanical properties of a shale formation: middle and upper devonian Horn River Group shale, northeast British Columbia, Canada. *AAPG Bull.* 101, 177–204.
- Dong, T., Harris, N.B., Knapp, L.J., McMillan, J.M., Bish, D.L., 2018. The effect of thermal maturity on geomechanical properties in shale reservoirs: an example from the Upper Devonian Duvernay Formation, Western Canada Sedimentary Basin. *Mar. Petrol. Geol.* 97, 137–153.
- Ducros, M., Sassi, W., Vially, R., Euzen, T., Crombez, V., 2017. 2-d basin modeling of the western Canada sedimentary basin across the montney-doig system: implications for hydrocarbon migration pathways and unconventional resources potential. In: AbuAli, Mahdi A., Moretti, Isabelle, Hege, M., Bolås, Nordgård (Eds.), *Petroleum Systems Analysis—Case Studies*, vol. 114. AAPG Memoir, pp. 117–134.
- Ejezie, N., 2007. Triassic Oil Families and Possible Source Rocks, Peace River Embayment Area, Alberta, Canada. Master Thesis, University of Calgary, Alberta, Canada, p. 393.
- Engelder, T., Fischer, M.P., 1994. Influence of poroelastic behavior on the magnitude of minimum horizontal stress,  $S_h$  in overpressured parts of sedimentary basins. *Geology* 22 (10), 949–952.
- Engelder, T., Peacock, D.C., 2001. Joint development normal to regional compression during flexural-flow folding: the Lillstock buttress anticline, Somerset, England. *J. Struct. Geol.* 23 (2–3), 259–277.
- Engelder, T., Lash, G.G., Uzcátegui, R.S., 2009. Joint sets that enhance production from middle and upper devonian gas shales of the appalachian basin. *AAPG Bull.* 93 (7), 857–889.
- Euzen, T., Everett, B., Power, M., Crombez, V., Rohais, S., Vaisblat, N., Baudin, F., 2015. Geological controls on reservoir properties of the Montney Formation in the Northeastern BC: an integration of sequence stratigraphy, organic geochemistry, quantitative mineralogy and petrophysical analysis. In: CSEG CWSL Joint Annual Convention. Calgary, Canada, 4–8 May 2015.
- Euzen, T., Moslow, T.F., Crombez, V., Rohais, S., 2018. Regional stratigraphic architecture of the Spathian deposits in Western Canada – implications for the Montney resource play. In: Euzen, T., Moslow, T.F., Caplan, M. (Eds.), *The Montney Play of Western Canada: Deposition to Development*, vol. 66. Bulletin of Canadian Petroleum Geology, pp. 175–192.
- Euzen, T., Watson, N., Fowler, M., Mort, A., Moslow, T.F., 2020. Petroleum distribution in the Montney hybrid play: source, carrier bed and structural controls. *AAPG (Am. Assoc. Pet. Geol.) Bull.*
- Fantle, M.S., Maher, K.M., DePaolo, D.J., 2010. Isotopic approaches for quantifying the rates of marine burial diagenesis. *Rev. Geophys.* 48, RG3002. <https://doi.org/10.1029/2009RG000306>.
- Faure, J.L., Osadetz, K., Benaoui, Z.N., Schneider, F., Roure, F., 2004. Kinematic and petroleum modeling of the Alberta foothills and adjacent foreland - west of Calgary. *Oil Gas Sci. Technol. - Rev. IFP* 59 (1), 81–108.
- Feng, W., Chen, Z., Jiang, C., 2016. Oil and Source Correlations of Triassic Montney Formation in WCSB: Implication to Shale Gas Resource Potential. *Geoconvention, Calgary*, March 2016.
- Feng, W., Chen, Z., Jiang, C., Harris, N., 2017. Volumetric Method to Determine the Contribution of Montney Sourced Hydrocarbons to the Montney and Doig Petroleum System. *Geoconvention, Calgary*, March 2017.
- Ferri, F., Zonneveld, J.P., 2008. Were triassic rocks of the western Canada sedimentary basin deposited in a foreland. *Canadian Society of Petroleum Geologists Reservoir* 35 (10), 12–14.
- Ferrill, D.A., Morris, P., Evans, M.A., Burkhard, M., Groshong, R.H., Onasch, C.M., 2004. Calcite twin morphology: a low-temperature deformation geothermometer. *J. Struct. Geol.* 26 (8), 1521–1529.
- Fuentes, F., DeCelles, P.G., Constenius, K.N., Gehrels, G.E., 2011. Evolution of the Cordilleran foreland basin system in northwestern Montana. *U.S.A. Geological Society of America Bulletin* 123, 507–533. <https://doi.org/10.1130/B30204.1>.
- Furlong, C.M., Gingras, M.K., Moslow, T.F., Zonneveld, J.P., 2018a. The Sunset Prairie formation: designation of a new middle triassic formation between the lower triassic Montney formation and middle triassic Doig formation in the western Canada sedimentary basin, northeast British Columbia. *Bull. Can. Petrol. Geol.* 66 (1), 193–214.
- Furlong, C.M., Gogolick, A., Gingras, M.K., González, P., Moslow, T.F., Prenoslo, D., Playter, T., Zonneveld, J.P., 2018b. Sedimentology and ichnology of the middle triassic (anisian) Sunset Prairie formation of the western Canada sedimentary basin. *Bull. Can. Petrol. Geol.* 66 (1), 215–236.
- Gabellone, T., Gasparrini, M., Iannace, A., Invernizzi, C., Mazzoli, S., D’Antonio, M., 2013. Fluid channelling along thrust zones: the Lagonegro case history, Southern Apennines, Italy. *Geofluids* 13 (2), 140–158. <https://doi.org/10.1111/gfi.12020>.
- Gale, J.F.W., Holder, J., 2010. Natural fractures in some US shales and their importance for gas production. Geological Society, London, Petroleum Geology Conference Series 7, 1131–1140. <https://doi.org/10.1144/0071131>.
- Gale, J.F.W., Reed, R.M., Holder, J., 2007. Natural fractures in the Barnett Shale and their importance for hydraulic fracture treatments. *AAPG (Am. Assoc. Pet. Geol.) Bull.* 91 (4), 603–622.
- Gale, J.F.W., Laubach, S.E., Olson, J.E., Eichhubl, P., Fall, A., 2014. Natural fractures in shale: a review and new observations. *AAPG (Am. Assoc. Pet. Geol.) Bull.* 98 (11), 2165–2216.
- Gasparrini, M., Sassi, W., Gale, J.F.W., 2014. Natural sealed fractures in mudrocks: a case study tied to burial history from the Barnett Shale, Fort Worth Basin, Texas, USA. In: Lacombe, O., Swennen, R., Caracausi, A. (Eds.), *Fluid-rock-tectonics Interactions in Basins and Orogens, Special Issue*, vol. 55, pp. 122–141. <https://doi.org/10.1016/j.marpetgeo.2013.12.006>. Marine and Petroleum Geology.
- Gasparrini, M., López-Cilla, I., Blázquez-Fernández, S., Rosales, I., Lerat, O., Martín-Chivelet, J., Doligez, B., 2017. A multidisciplinary modeling approach to assess facies-dolomitization-porosity interdependence in a Lower Cretaceous platform (northern Spain). In: MacNeil, A.J., Lonnee, J., Wood, R. (Eds.), “Characterization and Modeling of Carbonates—Mountjoy Symposium 1”, *SEPM Special Publication* 109. SEPM (Society for Sedimentary Geology), Tulsa, Oklahoma, pp. 130–153. <https://doi.org/10.2110/sepsp.109.07>.
- Ghanizadeh, A., Clarkson, C.R., Aquino, S., Ardakani, O.H., Sanei, H., 2015. Petrophysical and geomechanical characteristics of Canadian tight oil and liquid-rich gas reservoirs: I. Pore network and permeability characterization. *Fuel* 153, 664–681.
- Ghanizadeh, A., Clarkson, C.R., Aquino, S., Ardakani, O.H., Sanei, H., 2015. Petrophysical and geomechanical characteristics of Canadian tight oil and liquid-rich gas reservoirs: II. Geomechanical property estimation. *Fuel* 153, 682–691.
- Gillen, K., Wood, J.M., Sharp, L., Grimison, T., Guerard, B., 2019. Natural and induced structural fabrics in drill cores from the Montney formation. In: *New Directions in Geosciences for Unconventional Resources, 2019 William C. Gussow Geoscience Conference*, Calgary, Alberta, 15–17 October, 2019.
- Gillespie, J.M., Heller, P.L., 1995. Beginning of foreland subsidence in the Columbian-Seqvior belts. southern Canada and northwest Montana. *Geology* 23, 723–726. [https://doi.org/10.1130/0091-7613\(1995\)023<0723:BOFSIT>2.3.CO;2](https://doi.org/10.1130/0091-7613(1995)023<0723:BOFSIT>2.3.CO;2).
- Golding, M.L., Orchard, M.J., Zonneveld, J.P., Wilson, N.S.F., Reinson, G., 2015. Determining the age and depositional model of the Doig Phosphate Zone in northeastern British Columbia using conodont biostratigraphy. *Bull. Can. Petrol. Geol.* 63 (2), 143–170.
- Hans, U., Kleine, T., Bourdon, B., 2013. Rb–Sr chronology of volatile depletion in differentiated protoplanets: BABI, ADOR and ALL revisited. *Earth Planet Sci. Lett.* 374, 204–214. <https://doi.org/10.1016/j.epsl.2013.05.029>.
- Hansman, R.J., Albert, R., Gerdes, A., Ring, U., 2018. Absolute ages of multiple generations of brittle structures by U–Pb dating of calcite. *Geology* 46, 207–210.
- Hardebol, N., Callot, J.-P., Bertotti, J.L., Faure, J.L., 2009. Sedimentary and tectonic burial history appraisal and consequent temperature and organic maturation evolution in thrust-belt systems: a study on the SE Canadian Cordillera. *Tectonics* 28, TC3003. <https://doi.org/10.1029/2008TC002>.
- Higley, D.K., Henry, M.E., Roberts, L.N.R., 2005. Petroleum system modeling of the western Canada sedimentary basin-isopach Grid files. US Geological Survey. Open-File. <https://doi.org/10.3133/ofr20051421>. Report 2005-1421.
- Honlet, R., Gasparrini, M., Mueche, P., Swennen, R., John, C., 2018. A novel approach to geobarometry by combining fluid inclusion and clumped isotope ( $\Delta_{47}$ ) thermometry in hydrothermal carbonates. *Terra. Nova* 30 (3), 199–206. <https://doi.org/10.1111/ter.12326>.
- Hooker, J.N., Huggett, J.M., Cartwright, J., Ali Hussein, M., 2017a. Regional-scale development of opening-mode calcite veins due to silica diagenesis. *Geochem. Geophys. Geosyst.* 18.
- Hooker, J.N., Cartwright, J., Stephenson, B., Silver, C.R.P., Dickson, A.J., Hsieh, Y.-T., 2017b. Fluid evolution in fracturing black shales, Appalachian Basin. *AAPG Bull.* 101 (8), 1203–1238. <https://doi.org/10.1306/10031616030>.
- Hooker, J.N., Abu-Mahfouza, I.S., Meng, Q., Cartwright, J., 2019. Fractures in mudrocks: advances in constraining timing and understanding. *J. Struct. Geol.* 125, 166–173. <https://doi.org/10.1016/j.jsg.2018.04.020>.
- Hooker, J.N., Ruhl, M., Dickson, A.J., Hansen, L.N., Idiz, E., Hesselbo, S.P., Cartwright, J., 2020. Shale anisotropy and natural hydraulic fracture propagation: an example from the Jurassic (Toarcian) Posidonienschiefer, Germany. *J. Geophys. Res.: Solid Earth* 125, e2019JB018442. <https://doi.org/10.1029/2019JB018442Hu>.
- Ibrahim, A., Riediger, C.L., 2004. Hydrocarbon Source Rock Potential as Determined by Rock-Eval 6/TOC Pyrolysis, NEBC and NW Alberta: Resource Development and Geoscience Branch, Summary of Activities 2004. British Columbia Ministry of Energy and Mines, pp. 7–17 <http://www.empr.gov.bc.ca/OG/oilandgas/petroleumgeology/ConventionalOilAndGas>.
- Ilgel, A.G., Heath, J.E., Akkuttu, I.Y., Bryndzia, L.T., Cole, D.R., Kharaka, Y.K., Kneafsey, T.J., Milliken, K.L., Pyrak-Nolte, L.J., Suarez-Rivera, R., 2017. Shales at all scales: exploring coupled processes in mudrocks. *Earth Sci. Rev.* 166, 132–152.
- Jarvie, D.M., Hill, R.J., Ruble, T.E., Pollastro, R.M., 2007. Unconventional shale-gas systems: the Mississippian Barnett Shale of north-central Texas as one model for thermogenic shale-gas assessment. *AAPG (Am. Assoc. Pet. Geol.) Bull.* 91, 475–499.

- Jochum, J., Friedrich, G., Leythaeuser, D., Littke, R., Ropertz, B., 1995. Hydrocarbon-bearing fluid inclusions in calcite-filled horizontal fractures from mature Posidonia Shale (Hils Syncline, NW Germany). *Ore Geol. Rev.* 9, 363–370.
- Khalifa, M., Gasparri, M., 2014. Open versus closed mesogenetic systems in Cretaceous tidal and fluvial sandstones, Sirt Basin, Libya. *GeoArabia* 19 (4), 113–140.
- Kyser, T.K., Hiatt, E.E., Renac, C., Durocher, K., Holk, G.J., Deckart, K., 2000. Diagenetic fluids in paleo- and meso-Proterozoic sedimentary basins and their implications for long protracted fluid histories. In: Kyser, K. (Ed.), *Fluids and Basin Evolution*, vol. 262. Mineralogical Association of Canada, Ottawa, Canada, pp. 225–262. <https://doi.org/10.13140/2.1.1033.1847>.
- Labani, M.M., Rezaee, R., 2015. The importance of geochemical parameters and shale composition on rock mechanical properties of gas shale reservoirs: a case study from the Kockatea Shale and Carynginia Formation from the Perth Basin, Western Australia. *Rock Mech. Rock Eng.* 48 (3), 1249–1257.
- Lacombe, O., 2010. Calcite twins, a tool for tectonic studies in thrust belts and stable orogenic forelands. *Oil and Gas Science and Technology, Rev. IFP* 65 (6), 809–838.
- Lafargue, E., Marquis, F., Pillot, D., 1998. Rock-eval 6 applications in hydrocarbon exploration, production, and soil Contamination studies. *OGST, Rev. IFP* 53 (4), 421–437. <https://doi.org/10.2516/ogst:1998036>.
- Laubach, S.E., 2003. Practical approaches to identifying sealed and open fractures. *AAPG (Am. Assoc. Pet. Geol.) Bull.* 87 (4), 561–579.
- Lazar, O.R., Bohacs, K.M., Macquaker, J.H.S., Schieber, J., Demko, T.M., 2015. Capturing key attributes of fine-grained sedimentary rocks in outcrops, cores, and thin sections: nomenclature and description guidelines. *J. Sediment. Res.* 85, 230–246. <https://doi.org/10.2110/jsr.2015.11>, 2015.
- Liseroudi, M.H., Ardakani, O.H., Sanei, H., Pedersen, P.K., Stern, R.A., Wood, J.M., 2020. Origin of sulfate-rich fluids in the early triassic Montney formation, western Canadian sedimentary basin. *Mar. Petrol. Geol.* 114 (104236), 1–17. <https://doi.org/10.1016/j.marpetgeo.2020.104236>.
- Mangenot, X., Bonifacie, M., Gasparri, M., Götz, A., Ader, M., Rouchon, V., 2017. Coupling  $\Delta_{47}$  and fluid inclusion thermometry on carbonate cements to precisely reconstruct the temperature, salinity and  $\delta^{18}\text{O}$  of paleo-groundwater in sedimentary basins. *Chem. Geol.* 472, 44–57. <https://doi.org/10.1016/j.chemgeo.2017.10.011>.
- Mangenot, X., Gasparri, M., Gerdes, A., Bonifacie, M., Rouchon, V., 2018. An emerging thermo-chronometer for carbonate bearing-rocks:  $\Delta_{47}(\text{U-Pb})$ . *Geology* 46 (12), 1067–1070. <https://doi.org/10.1130/G45196.1>.
- Marquez, X.M., Mountjoy, E.W., 1996. Microcracks due to overpressures caused by thermal cracking in well-sealed Upper Devonian reservoirs, deep Alberta basin. *AAPG (Am. Assoc. Pet. Geol.) Bull.* 80, 570–588.
- McCaig, A.M., Knipe, R.J., 1990. Mass-transport mechanisms in deforming rocks: recognition using microstructural and microchemical criteria. *Geology* 18, 824–827.
- McKean, S.H., Priest, J.A., 2019. Multiple failure state triaxial testing of the Montney Formation. *J. Petrol. Sci. Eng.* 173, 122–135.
- McLimans, R.K., 1987. The application of fluid inclusions to migration of oil and diagenesis in petroleum reservoirs. *Appl. Geochem.* 2 (5–6), 585–603.
- Meng, Q., Hooker, J.N., Cartwright, J., 2017. Early overpressuring in organic-rich shales during burial: evidence from fibrous calcite veins in the Lower Jurassic Shales-with-Beef Member in the Wessex Basin. *Journal of the Geological Society* 174 (5), 869–882. <https://doi.org/10.1144/jgs2016-146>.
- Miall, A.D., Cataneanu, O., Vakarelov, B.K., Post, R., 2008. The western interior basin. In: Miall, A.D. (Ed.), *The Sedimentary Basins of the United States and Canada. Sedimentary Basins of the World 5*. Elsevier Science, Amsterdam, Netherlands, pp. 329–362. [https://doi.org/10.1016/S1874-5997\(08\)00009-9](https://doi.org/10.1016/S1874-5997(08)00009-9).
- Morad, S., Ketzler, J.M., De Ros, L.F., 2002. Spatial and temporal distribution of diagenetic alterations in siliclastic rocks: implications for mass transfer in sedimentary basins. *Sedimentology* 47 (1), 95–120. <https://doi.org/10.1046/j.1365-3091.2000.00007.x>.
- Moslow, T.F., 2000. Reservoir architecture of a fine-grained turbidite system: lower triassic Montney formation, western Canada sedimentary basin. In: Weimer, P., Slatt, R.M., Coleman, J., Rosen, N.C., Nelson, H., Bouma, A.H., Styzen, M.J., Lawrence, D.T. (Eds.), *Deep-water Reservoirs of the World, Conference Proceedings, Gulf Coast, SEP.M.*, pp. 686–713.
- Moslow, T.F., Adams, M.G., Terzuoli, T., 2016. Bioclastic reservoirs of the distal Montney "shale" play. In: AAPG 2016 Annual Convention and Exhibition, Calgary, Alberta, Canada, June 16–22, 2016. AAPG Search and Discovery, p. 13. Article #80548.
- Moslow, T.F., Haverslew, B., Hendersen, C.M., 2018. Sedimentary facies, petrology, reservoir characteristics, conodont biostratigraphy and sequence stratigraphic framework of a continuous (395m) full diameter core of the Lower Triassic Montney Fm., northeastern British Columbia. In: Euzen, T., Moslow, T.F., Caplan, M. (Eds.), *The Montney Play: Deposition to Development*, vol. 66. Bulletin of Canadian Petroleum Geology, pp. 259–287, 1.
- Mossop, G.D., Shetsen, I., 1994. Geological Atlas of the Western Canada Sedimentary Basin. Canadian Society of Petroleum Geologists and Alberta Research Council. <http://ags.aer.ca/reports/atlas-of-the-western-canada-sedimentary-basin.htm>.
- Ness, S.M., 2001. The Application of Basin Analysis to the Triassic Succession, Alberta Basin: an Investigation of Burial and Thermal History and Evolution of Hydrocarbons in Triassic Rocks. M. Sc. Thesis. University of Calgary, Calgary, Alberta, p. 179. <http://dspace.ucalgary.ca/handle/1880/40896>.
- O'Neil, J.R., 1969. Equilibrium and nonequilibrium oxygen isotope effects in synthetic carbonates. *Geochem. Cosmochim. Acta* 61, 3461–3475.
- Orchard, M.J., Zonneveld, J.P., 2009. The lower triassic sulphur mountain formation in the wapiti lake area: lithostratigraphy, conodont biostratigraphy, and a new biozonation for the lower olenekian (smithian) earth science sector (ESS) contribution 20080714. *Can. J. Earth Sci.* 46 (10), 757–790.
- Ozkaya, I., 1988. A simple analysis of oil-induced fracturing in sedimentary rocks. *Mar. Petrol. Geol.* 5 (3), 293–297.
- Panã, D.I., van der Pluijm, B.A., 2015. Orogenic pulses in the Alberta Rocky Mountains: radiometric dating of major faults and comparison with the regional tectono-stratigraphic record. *GSA Bulletin* 127 (3–4), 480–502.
- Parrish, R.R., Parrish, C.M., Lasalle, S., 2018. Vein calcite dating reveals Pyrenean orogen as cause of Paleogene deformation in southern England. *J. Geol. Soc.* 175, 425–442.
- Pauthier, S., Ducros, M., Chauveau, B., Euzen, T., Sassi, W., 2016. Modeling source rock distribution, thermal maturation, petroleum retention and expulsion: The Case of the Western Canadian Sedimentary Basin (WCSB). In: AAPG Hedberg Conference, The Future of Basin and Petroleum Systems Modeling, Santa Barbara, California, USA, April 3–6 2016.
- Peacock, D.C.P., Mann, A., 2005. Evaluation of the controls on fracturing in reservoir rocks. *J. Petrol. Geol.* 28 (4), 385–396.
- Pei, P., He, J., Ling, K., 2014. Correlating geomechanical properties of the bakken formation rocks with lithofacies and sequence. In: 48th US Rock Mechanics/ Geomechanics Symposium. American Rock Mechanics Association.
- Pei, P., Ling, K., Hou, X., Nordeng, S., Johnson, S., 2016. Brittleness investigation of producing units in Three Forks and Bakken formations, Williston basin. *J. Nat. Gas Sci. Eng.* 32, 512–520.
- Peirce, J.W., Cordsen, A., Glenn, T., 2001. The Great Slave Lake Shear Zone—Implications for Exploration in NW Alberta and NE British Columbia. Canadian Society of Exploration Geophysicists Convention.
- Peng, J., Milliken, K.M., Qilong, F., 2020. Quartz types in the Upper Pennsylvanian organic-rich Cline Shale (Wolfcamp D), Midland Basin, Texas: implications for silica diagenesis, porosity evolution and rock mechanical properties. *Sedimentology* 67, 2040–2064. <https://doi.org/10.1111/sed.12694>.
- Perez, R., Marfurt, K., 2013. Calibration of Brittleness to elastic rock properties via mineralogy logs in unconventional reservoirs. International Conference and Exhibition of American Association of Petroleum Geologists (AAPG), Cartagena, Sept. 8–11. Article #41237.
- Playter, T., Corlett, H., Konhauser, K., Robbins, L., Rohais, S., Crombez, V., Maccormack, K., Rokosh, D., Prenoslo, D., Furlong, C.M., Pawlowicz, J., Gingras, M., Lalonde, S., Lyster, S.N., Zonneveld, J.P., 2018. Clinof orm identification and correlation in fine-grained sediments: a case study using the Triassic Montney Formation. *Sedimentology* 65 (1), 263–302. <https://doi.org/10.1111/sed.12403>.
- Price, R.A., 1994. Cordilleran tectonics and the evolution of the Western Canada sedimentary basin. In: Mossop, G. (Ed.), *Shetsen, I., Compilers, Geological Atlas of the Western Canada Sedimentary Basin*. Canadian Society of Petroleum Geologists and Alberta Research Council, pp. 13–24.
- Quesnel, B., Boulvais, P., Gautier, P., Cathelineau, M., John, C.M., Dierick, M., Agrinier, P., Drouillet, M., 2016. Paired stable isotopes (O, C) and clumped isotopothermometry of magnesite and silica veins in the New Caledonia Peridotite Nappe. *Geochem. Cosmochim. Acta* 183, 234–249.
- Ramsay, J.G., 1980. The crack-seal mechanism of rock deformation. *Nature* 284, 135–139.
- Riazi, N., Clarkson, C.R., Ghanizadeh, A., Vahedian, A., Aquino, S., Wood, J.M., 2017. Determination of elastic properties of tight rocks from ultrasonic measurements: examples from the Montney Formation (Alberta, Canada). *Fuel* 196, 442–457.
- Riediger, C.L., 1997. Geochemistry of potential hydrocarbon source rocks of Triassic age in the Rocky Mountain Foothills of northeastern British Columbia and west-central Alberta. *Bull. Can. Petrol. Geol.* 45 (4), 719–741.
- Riediger, C.L., Brooks, P.W., Fowler, M.G., Snowdon, L.R., 1990a. Lower and Middle Triassic source rocks, thermal maturation, and oil-source rock correlations in the Peace River Embayment area, Alberta and British Columbia. *Bull. Can. Petrol. Geol.* 38A, 218–235.
- Riediger, C.L., Fowler, M.G., Brooks, P.W., Snowdon, L.R., 1990b. Triassic oils and potential mesozoic source rocks, Peace River Arch area, western Canada basin. *Org. Geochem.* 16, 295–305.
- Rijken, P., Cooke, M.L., 2001. Role of shale thickness on vertical connectivity of fractures: application of crack-bridging theory to the Austin Chalk, Texas. *Tectonophysics* 337 (1–2), 117–133.
- Rohais, S., Crombez, V., Euzen, T., Zonneveld, J.-P., 2018. Subsidence dynamics of the Montney formation (early triassic, western Canada sedimentary basin): insights for its geodynamic setting and wider implications. In: Euzen, T., Moslow, T.F., Caplan, M. (Eds.), *The Montney Play of Western Canada: Deposition to Development*, vol. 66. Bulletin of Canadian Petroleum Geology, pp. 128–160.
- Romero-Sarmiento, M.F., Ducros, M., Carpentier, B., Lorient, F., Cacas, M.-C., Pegaz-Fiornet, S., Wolf, S., Rohais, S., Moretti, I., 2013. Quantitative evaluation of TOC, organic porosity and gas retention distribution in a gas shale play using petroleum system modeling: application to the Mississippian Barnett shale. *Mar. Petrol. Geol.* 45, 315–330. <https://doi.org/10.1016/j.marpetgeo.2013.04.003>.
- Romero-Sarmiento, M.F., Pillot, D., Letort, G., Lamoureux-Var, V., Beaumont, V., Huc, A.Y., Garcia, B., 2016a. New Rock-Eval method for characterization of unconventional shale resource systems. *Oil & Gas Science and Technology—Revue d'IFP Energies nouvelles* 71 (3), 37.
- Romero-Sarmiento, M.F., Euzen, T., Rohais, S., Jiang, C., Littke, R., 2016b. Artificial thermal maturation of source rocks at different thermal maturity levels: application to the Triassic Montney and Doig formation in the Western Canada sedimentary basin. *Org. Geochem.* 97, 148–162. <https://doi.org/10.1016/j.orggeochem.2016.05.002>.
- Roure, F., Swennen, R., Schneider, F., Faure, J.L., Ferket, H., Guilhaumou, N., Osadet, K., Robion, P., Vandeginst, V., 2005. Incidence and importance of tectonics and natural fluid migration on reservoir evolution in foreland fold-and-thrust belts. *Oil & Gas Science and Technology - Revue de l'IFP* 60 (60), 67–106. <https://doi.org/10.2516/ogst:2005006>.
- Roure, F., Callot, J.P., Faure, J.L., Ferket, H., Gonzales, E., Guilhaumou, N., Lacombe, O., Malandain, J., Sassi, W., Schneider, F., Swennen, R., Vilasi, N., 2010. The use of

- palaeo-thermo-barometers and coupled thermal, fluid flow and pore-fluid pressure modeling for hydrocarbon and reservoir prediction in fold and thrust belts. Geological Society of London, Special Publication 348, 87–114.
- Rybacki, E., Reinicke, A., Meier, T., Makasi, M., Dresen, G., 2015. What controls the mechanical properties of shale rocks?—Part I: strength and Young's modulus. *J. Petrol. Sci. Eng.* 135, 702–722.
- Rybacki, E., Meier, T., Dresen, G., 2016. What controls the mechanical properties of shale rocks?—Part II: Brittleness. *J. Petrol. Sci. Eng.* 144, 39–58.
- Sanders, S., Etienne, C., Gegolick, A., Kelly, D., Zonneveld, J.-P., 2018. The Middle Montney Altares Member: lithology, depositional setting and significance for horizontal drilling and completion in the Altares Field, British Columbia. In: Euzen, T., Moslow, T.F., Caplan, M. (Eds.), *The Montney Play: Deposition to Development*, vol. 66. Bulletin of Canadian Petroleum Geology, pp. 318–337, 1.
- Sanei, H., Wood, J.M., Ardakani, O.H., Clarkson, C.R., Jiang, C., 2015. Characterization of organic matter fractions in an unconventional tight gas siltstone reservoir. *Int. J. Coal Geol.* 150, 296–305.
- Sassi, W., Milelli, L., Gasparri, M., 2013. Fracturing in Basin Models, Application to the Barnett Formation in the Fort Worth Basin, Texas. AAPG Annual Convention and Exhibition, Pittsburgh, Pennsylvania. Search and Discovery Article #10594.
- Sibley, D.F., Gregg, J.M., 1987. Classification of dolomite rock textures. *J. Sediment. Res.* 57 (6).
- Spencer, C.W., 1987. Hydrocarbon generation as a mechanism for overpressuring in Rocky Mountain region. AAPG (Am. Assoc. Pet. Geol.) Bull. 71, 368–388.
- Swart, P., 2015. The geochemistry of carbonate diagenesis: the past, present and future. *Sedimentology* 62 (5), 1233–1304. <https://doi.org/10.1111/sed.12205>.
- Tavani, S., Storti, F., Lacombe, O., Corradetti, A., Muñoz, J., Mazzoli, S., 2015. A review of deformation pattern templates in foreland basin systems and fold-and-thrust belts: implications for the state of stress in the frontal regions of thrust wedges. *Earth Sci. Rev.* 141, 82–104.
- Tufano, B.C., Pietras, J.T., 2017. Coupled flexural-dynamic subsidence modeling approach for retroforeland basins: example from the Western Canada Sedimentary Basin. *GSA Bulletin* 129 (11/12), 1622–1635.
- Ukar, E., Lopez, R.G., Gale, J.F.W., Laubach, S.E., Manceda, R., 2017. New type of kinematic indicator in bed-parallel veins, late Jurassic/Early Cretaceous vaca muerta formation, Argentina: E-W shortening during late Cretaceous vein opening. *J. Struct. Geol.* 104, 31–47.
- Vaisblat, N., 2020. Controls on Reservoir Quality in the Lower Triassic Montney Formation. PhD thesis. University of Alberta (Canada), p. 286.
- Vaisblat, N., Ayranci, K., Harris, N., 2017a. Is siltstone geomechanics on the mixing line between sandstone and shale? Example from the western Canada sedimentary basin Montney formation. In: AAPG Annual Convention and Exhibition.
- Vaisblat, N., Harris, N.B., DeBhur, C., Euzen, T., Gasparri, M., Crombez, V., Ayranci, K., 2017b. Diagenetic Model for the Deep Montney Formation, Northeastern British Columbia. *Geoscience BC Summary of Activities 2016*, 2017-1.
- Vaisblat, N., Rangriz Shokri, A., Ayranci, K., Harris, N., Chalaturnyk, R.J., 2019. Significance of rock compositional control on geomechanical properties and hydraulic fracturing of the Montney formation, western Canadian basin. Unconventional Resources Technology Conference. <https://doi.org/10.15530/AP-URTEC-2019-198199>.
- Van de Kamp, P.C., 2008. Smectite-illite-muscovite transformations, quartz dissolution, and silica release in shales. *Clay Clay Miner.* 56, 66–81.
- Van den Kerkhof, A., Thiery, R., 2001. Carbonic inclusions. *Lithos* 55 (1), 49–68.
- Vandeginste, V., Swennen, R., Faure, J.-L., Osadetz, K., Roure, F., 2012. Paleostress evolution in the Canadian Cordilleran foreland fold-and-thrust belt west of Calgary». *Geol. Belg.* 15 (1–2), 42–52. <https://popups.uliege.be/443/1374-8505/index.php?id=3505>.
- Veizer, J., Ala, D., Azmy, K., Bruckschen, P., Buhl, D., Bruhn, F., Jasper, T., 1999.  $^{87}\text{Sr}/^{86}\text{Sr}$ ,  $\delta^{13}\text{C}$  and  $\delta^{18}\text{O}$  evolution of Phanerozoic seawater. *Chem. Geol.* 161 (1), 59–88.
- Vernik, L., 1994. Hydrocarbon-generation-induced microcracking of source rocks. *Geophysics* 59 (4), 555–563.
- Vishkai, M., Wang, J., Wong, R.C.K., Clarkson, C.R., Gates, I.D., 2017. Modeling geomechanical properties in the Montney formation, Alberta, Canada. *Int. J. Rock Mech. Min. Sci.* 96, 94–105.
- Wang, F.P., Gale, J.F.W., 2009. Screening criteria for shale-gas systems. *Gulf Coast Assoc. Geol. Soc. Trans.* 59, 779–793.
- Wang, R., Ding, W., Zhang, Y., Wang, Z., Wang, X., He, J., Zeng, W., Dai, P., 2016. Analysis of developmental characteristics and dominant factors of fractures in Lower Cambrian marine shale reservoirs: a case study of Niutitang formation in Cen'gong block, southern China. *J. Petrol. Sci. Eng.* 138, 31–49. <https://doi.org/10.1016/j.petrol.2015.12.004>.
- Wang, X., Wang, R., Ding, W., Yin, S., Sun, Y., Zhou, X., Li, Q., 2017. Development characteristics and dominant factors of fractures and their significance for shale reservoirs: a case study from E1b2 in the Cen'gong block, southern China. *J. Petrol. Sci. Eng.* 159, 988–999.
- Wood, J.M., Saney, H., Curtis, M.E., Clarkson, C.R., 2015. Solid bitumen as a determinant of reservoir quality in an unconventional tight gas siltstone play. *Int. J. Coal Geol.* 150, 287–295.
- Wood, J.M., Ardakani, O.H., Saney, H., Curtis, M.E., Royer, D., 2020. Application of paleoporosity and bitumen saturation concepts to tight-gas accumulations containing solid bitumen. *Int. J. Coal Geol.* 228, 103547.
- Woodcock, N.H., Dickson, J.A.D., Tarasewicz, J.P.T., 2007. Transient permeability and reseat hardening in fault zones: evidence from dilation breccia textures. *Geological Society, London, Special Publications* 270 (1), 43–53.
- Wright, G.N., McMechan, M.E., Potter, D.E.G., 1994. Structure and architecture of the western Canada sedimentary basin. In: Mossop, G.D., Shetsen, I. (Eds.), *Geological Atlas of the Western Canada Sedimentary Basin*. CSPG and Alberta Research Council, pp. 25–40.
- Yasin, Q., Du, Q., Sohail, G.M., Ismail, A., 2017. Impact of organic contents and brittleness indices to differentiate the brittle-ductile transitional zone in shale gas reservoir. *Geosci. J.* 21 (5), 779–789.
- Zanella, A., Cobbold, P.R., Rojas, L., 2014. Beef Veins and Thrust Detachments in Early Cretaceous Source Rocks, Foothills of Magallanes-Austral Basin, Southern Chile and Argentina: Structural Evidence for Fluid Overpressure during Hydrocarbon Maturation.
- Zeng, W., Zhang, J., Ding, W., Zhao, S., Zhang, Y., Liu, Z., Jiu, K., 2013. Fracture development in Paleozoic shale of Chongqing area (South China). Part one: fracture characteristics and comparative analysis of main controlling factors. *J. Asian Earth Sci.* 75, 251–266.
- Zonneveld, J.P., Moslow, T.F., 2018. Palaeogeographic setting, lithostratigraphy, and sedimentary framework of the lower triassic Montney formation of western Alberta and northeastern British Columbia. *Bull. Can. Petrol. Geol.* 66 (1), 93–127.
- Zonneveld, J.P., Moslow, T.F., Henderson, C.M., 1997. Lithofacies associations and depositional environments in a mixed siliciclastic-carbonate coastal depositional system, upper Liard Formation, Triassic, northeastern British Columbia. *Bull. Can. Petrol. Geol.* 45 (4), 553–575.
- Zonneveld, J.P., Gingras, M.K., Pemberton, S.G., 2001. Trace fossil assemblages in a Middle Triassic mixed siliciclastic-carbonate marginal marine depositional system, British Columbia. *Palaeogeogr. Palaeoclimatol. Palaeoecol.* 166 (3–4), 249–276.